AGU Advances

Original Version of

Marginal reefs under stress: physiological limits render Galápagos corals susceptible to ocean acidification and thermal stress

Diane Thompson[1], Malcolm McCulloch[2], Julia E. Cole[3], Emma V. Reed[1], Juan P. D'Olivo[4], Kelsey Dyez[3], Marcus Lofverstrom[1], Janice Lough[5,6], Neal Cantin[5], Alexander W. Tudhope[7], Anson H. Cheung[8], Lael Vetter[1], R. Lawrence Edwards[9]

[1] University of Arizona, Department of Geosciences, Tucson, 85721, USA
[2] University of Western Australia, ARC Centre of Excellence for Coral Reefs Studies, Oceans Graduate School and Oceans Institute, Crawley, 6009, Australia
[3] University of Michigan, Earth and Environmental Sciences, Ann Arbor, 48109, USA
[4] Freie Universität Berlin, Berlin, 12249, Germany
[5] Australian Institute of Marine Science, PMB 3, Townsville MC, Queensland 4810, Australia
[6] ARC Centre of Excellence for Coral Reef Studies, James Cook University, Townsville, Queensland 4811, Australia
[7] University of Edinburgh, School of Geosciences, Edinburgh EH9 3JW, UK
[8] Department of Earth, Environmental, and Planetary Sciences, Brown University, Providence, RI 02912
[9] Department of Earth Sciences, University of Minnesota, Minneapolis, MN

Marginal reefs under stress: physiological limits render Galápagos corals susceptible to ocean acidification and thermal stress;

Short title: Physiological limits to corals' buffering capacity

Diane Thompson,[1*] Malcolm McCulloch,[2] Julia E. Cole,[3] Emma V. Reed,[1] Juan P. D'Olivo,[4] Kelsey Dyez,[3] Marcus Lofverstrom,[1] Janice Lough,[5,6] Neal Cantin,[5] Alexander W. Tudhope,[7] Anson H. Cheung,[8] Lael Vetter,[1] R. Lawrence Edwards[9]

[1]University of Arizona, Department of Geosciences, Tucson, 85721, USA
[2]University of Western Australia, ARC Centre of Excellence for Coral Reefs Studies,Oceans Graduate School and Oceans Institute, Crawley, 6009, Australia
[3]University of Michigan, Earth and Environmental Sciences, Ann Arbor, 48109, USA
[4]Freie Universität Berlin, Berlin, 12249, Germany
[5]Australian Institute of Marine Science, PMB 3, Townsville MC, Queensland 4810, Australia
[6]ARC Centre of Excellence for Coral Reef Studies, James Cook University, Townsville, Queensland 4811, Australia
[7]University of Edinburgh, School of Geosciences, Edinburgh EH9 3JW, U.K.
[8]Department of Earth, Environmental, and Planetary Sciences, Brown University, Providence, RI 02912
[9]Department of Earth Sciences, University of Minnesota, Minneapolis, MN

Key Points:

- Saturation of the internal growth medium is reduced in modern Galápagos *Porites* species corals, particularly following warm extremes.
- Corals display similar capacity to regulate their growth medium among sites and time periods, with limited adaptation to acidification.
- Taken together, these results suggest strict physiological limits to corals' ability to buffer against changing ocean conditions.

Corresponding author: Diane M. Thompson, thompsod@arizona.edu

Abstract

Ocean acidification and thermal stress may undermine corals' ability to calcify and support diverse reef communities, particularly in marginal environments. Coral calcification depends on aragonite supersaturation (Ω) of the calcifying fluid (cf) from which the skeleton precipitates. Corals actively upregulate pH_{cf} relative to seawater to buffer against changes in temperature and dissolved inorganic carbon (DIC_{cf}), which together control Ω_{cf}. Here we assess the buffering capacity in modern and fossil corals from the Galápagos that have been exposed to sub-optimal conditions, extreme thermal stress, and accelerated rates of acidification. We demonstrate a significant decline in pH_{cf} and Ω_{cf} since the pre-industrial era, trends which are exacerbated during extreme warm years. These results suggest that there are likely physiological limits to corals' pH buffering capacity, and that these constraints render marginal reefs particularly susceptible to ocean acidification.

Plain Language Summary

Reef-building corals buffer their internal environment to permit rapid growth, which is critical for creating the structure and function of coral reefs. However, we demonstrate that there are finite limits to the ability of to regulate their internal chemistry to optimize growth. This limitation will leave corals susceptible to ocean warming and acidification, particularly in sub-optimal environments. Galápagos corals already display signs of stress and their ability to maintain an optimal internal growth environment from the 18^{th} century to today.

Introduction

The carbonate structures of coral reef ecosystems provide critical defenses against storm surge and sea-level rise, supporting billions of dollars of goods and services annually beyond their intrinsic value (Spalding et al., 2017), highlighting the need to understand how changing ocean conditions impact coral calcification. Thermal stress and ocean acidification (OA) diminish coral calcification, as shown in both experimental systems and Free Ocean CO_2 Enrichment (FOCE) experiments on natural reefs (Gattuso et al., 2014). Analyses of coral density variations in cores of massive corals also reveal trends in coral calcification through time (Lough, 2010). Collectively, these studies demonstrate spatially and temporally varying rates of calcification, with significant declines under recent extreme

warming events and OA. Corals in the Galápagos Archipelago have been disproportionately impacted (Glynn et al., 2018), due to both extreme El Niño-related warming (Glynn et al., 1988; Glynn, 2001) and highly variable upwelling and pH/saturation state (Manzello et al., 2008; Manzello, 2010). These "marginal" reefs exhibit low diversity and structural complexity (Darwin & Bonney, 1889; Cortés, 1997; Glynn, 2001; Manzello et al., 2008; Glynn et al., 2017), and are experiencing acidification at rates of around -0.0026 yr^{-1} (Sutton et al., 2014). Differential recovery rates along spatial pH gradients (Manzello et al., 2014) further demonstrate the importance of carbonate chemistry and calcification processes to reef health in this region. As CO_2 levels rise, changing patterns of OA and warming will increase the pressure on eastern equatorial Pacific and other marginal reef environments.

Therefore, a critical question remains: do corals have the adaptive capacity to maintain sustainable calcification in the face of increasingly stressful environmental conditions? Here, we leverage advances in biomineralization and boron isotope systematics to assess how changes in energy availability alter rates of calcification, the chemistry of the calcifying fluid, and the geochemistry of the carbonate skeleton (Box 1, Table S1). We use this understanding of coral biomineralization to elucidate the susceptibility of coral calcification to OA and to assess the adaptive capacity of Galápagos (*Porites* sp.) corals to changing ocean conditions.

In reef-building corals, calcification varies in response to internal (physiological) and external (environmental) factors, and maintenance of aragonite supersaturation in their calcifying fluid ($\Omega_{cf} \gg 1$) is the ultimate factor that permits supercalcification and buffers against changes in seawater chemistry (McCulloch et al., 2012). This state is achieved via upregulation of DIC and pH in response to changing environmental conditions. For example, during cooler seasons, corals upregulate pH_{cf} in response to a drop in metabolic (i.e., from zooxanthellar photosynthesis and coral respiration) DIC, resulting from reduced temperature and light (e.g., (D'Olivo & McCulloch, 2017; McCulloch et al., 2017; Ross et al., 2017, 2019)). Cool temperatures also slow calcification kinetics and reduce the buffering capacity of the coral calcifying fluid (hereafter "thermodynamic" factors, (Guo, 2019; Georgiou et al., 2015)). By upregulating pH_{cf}, corals maintain a nearly constant aragonite saturation state, shifting the carbonate reactions to favor carbonate ion during the winter months (Fig. 1) and preserving their ability to calcify despite large seasonal changes in DIC availability and temperature. Box 1 illustrates

the major controls on the geochemistry of the calcifying fluid. If these processes operate across species and reef environments, corals may be able to withstand changes in seawater pH.

However, our understanding of coral biomineralization processes largely depends on studies of modern massive corals from regions with relatively low seasonal and geochemical variability (Fig. 2a-b). Although a few studies have leveraged natural CO_2 seeps to study coral biomineralization under extreme conditions (Wall et al., 2016, 2019), corals likely respond differently to sharp spatial gradients compared to temporal variations. In many marginal reef environments, strong oceanographic variability and low aragonite saturation states make reef-building corals particularly susceptible to changing ocean conditions. Further, such marginal reefs provide a potential analogue of future reef patterns, as OA broadens the coverage of sub-optimal to marginal conditions.

Here, we capitalize on the large natural gradients across the Pacific in SST variability (Fig. 2a) and aragonite saturation state (Fig. 2b) to understand the range of coral responses to ongoing warming and acidification. We apply a multi-proxy, multi-site synthesis of coral geochemistry, backed by a novel Earth system modelling framework, to reconstruct and contextualize the impact of environmental stresses on calcification and resiliency in Galápagos corals. We leverage geochemical tracers of coral biomineralization (Table S-1)–skeletal B/Ca ($[CO_3^{-}]$), $\delta^{11}B$ (pH_{cf}), and U/Ca ($[CO_3^{-}]$)–that constrain the calcifying fluid chemistry, including the aragonite saturation that governs calcification rate (DeCarlo et al., 2018, 2015). We combine these with paleo-environmental tracers that primarily reflect factors external to the coral calcification environment (Table S-1): Sr/Ca (Beck et al., 1992; Corrège et al., 2000), Li/Mg (Hathorne et al., 2013; Montagna et al., 2014), and $\delta^{18}O$ (Weber & Woodhead, 1972) (all primarily controlled by SST); Ba/Ca (upwelling) (Shen et al., 1992); and $\delta^{13}C$ (upwelling, metabolic carbon / photosynthetic health) (Shen et al., 1992). These new recent (1976-2010) and fossil (1729-1733) Galápagos records (Wolf Island, 1^o23.15'N, 91^o49.90'W) significantly extend the data coverage prior to the industrial era, which we leverage to assess the capacity of corals to buffer against changing environmental conditions. We compare our new Galápagos results with published data from the Great Barrier Reef (McCulloch et al., 2017) to contextualize results from the marginal Galápagos reef environment–a comparatively cold, low-saturation, and highly variable environment. Finally, we establish a comprehensive spatiotemporal framework for these results using simulations of ocean biogeochemistry that extend from pre-industrial to modern (Fig. 2c), permitting the first cross-

Box 1. Overview of coral calcification and controls on calcifying fluid geochemistry.

Although we often think of corals as forming skeletons that directly reflect seawater chemistry, in fact corals produce their skeletons from a semi-isolated, geochemically modulated fluid, separated from seawater by a layered dermal structure. The tissue layer from which the skeleton is formed is termed the calicoblastic ectoderm, which is bathed in the calcifying fluid (cf). Here we identify the processes that control the transport of skeletal "building blocks" into the calcifying fluid and the resulting fluid geochemistry. These processes are governed by both physiological and environmental factors, and they determine the geochemistry of the skeleton (Figure 1).

1. Seawater chemistry, indicated in black, is the starting point from which the coral imports skeletal materials.
2. Passive transport (diffusion) or vacuole invagination bring seawater into the calcification environment (blue).
3. Active transport uses energy from respiration and zooxanthellar photosynthesis to drive a paracellular and trans-membrane active transport of ions. For example, alkalinity "pumps" (such as Ca-ATPase) enrich alkalinity of the fluid by transporting Ca^{2+}, $2Na^{+}$, or $2K^{+}$ while removing $2H^{+}$ (e.g., Cohen and McConnaughey 2003; Al-Horani et al., 2003; Zoccola et al., 2004; Tanaka et al., 2015). This pH increase drives the carbonate equilibrium towards CO_3^{2-}, increases alkalinity, and raises the aragonite supersaturation, enabling rapid calcification. The Ca-ATPase pump also increases the Sr^{2+} concentration of the calcifying fluid (Marchitto et al., 2018), due to strontium's similarity in size and charge to Ca^{2+}. Certain details of these active transport pathways remain obscure: although it is stimulated by light and most active during the day, it may not be energy limited (McCulloch et al. 2012), and the mechanistic links to metabolic DIC remain poorly understood (Furla et al., 2000; Zoccola et al., 2015). A strong inverse relationship between pH and DIC_{cf} (e.g., McCulloch et al., 2017) suggests that low DIC, rather than high energy, may trigger active pathways. Thus active transport can be important even when energy sources are reduced under cooler, low-light conditions. The interplay of metabolic energy supplies with external environmental stresses may vary among reef environments, and different factors may become limiting depending on these details.
4. Rayleigh fractionation alters the relative proportion of minor and trace cations to Ca in the calcifying fluid as calcification proceeds. The proxy-relevant cations Sr, Mg, Ba, Li, and U are incorporated into the coral skeleton at differing rates due to varying partitioning coefficients. Calcification preferentially incorporates Sr and Ba, and discriminates against Mg, Li, and U, relative to the proportion of these elements in the cf. The degree to which Rayleigh fractionation impacts the cf chemistry will depend on the balance between calcification rate, which increasingly fractionates cf chemistry, and replenishment of seawater, which brings cf chemistry back to environmental levels. The susceptibility of different elements to this process depends on the partitioning coefficient (K_D) between fluid and aragonite during calcification, with values <1 indicating exclusion from the skeleton and those >1, preferential uptake: K(Sr/Ca) ~ 1.1 (Gaetani et al., 2006; Marchitto et al., 2018), K(Mg/Ca) ~ 0.001 (Gaetani et al., 2006), K(Ba/Ca) ~2.3 (Gaetani et al., 2006), K(Li/Ca) ~ 0.0006 (Hathorne et al., 2013), K(U/CO3) ~ 0.3 (DeCarlo et al., 2015)].

Figure 1.

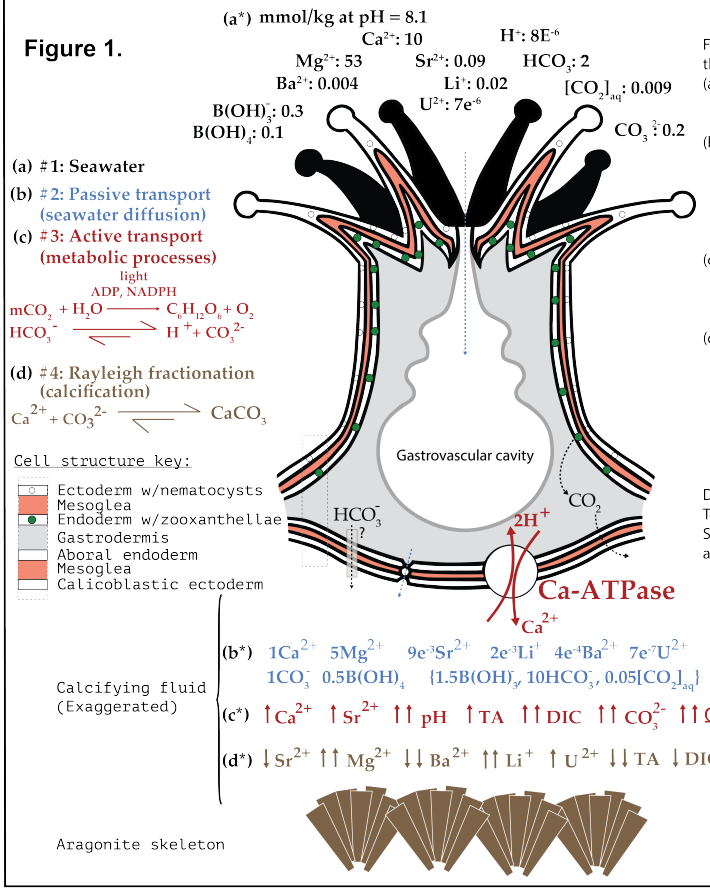

For major cations and anions in Figure 1, the notation is as follows:
(a*) concentration in seawater at a pH (total scale) of 8.1 (in mmol/kg, rounded to one significant figure);
(b*) as in (a*), due to 1:1 passive transport of ions, but now expressed as stoichiometric ratios with respect to 1 mole of $CaCO_3$ (ions in curly brackets are thought to play a minor role in coral carbonate reactions);
(c*) the relative impact of Ca-ATPase pump on calcifying fluid geochemistry, where known (McCulloch et al., 2017; Marchitto et al., 2018);
(d*) impact of calcification on the concentration of major cations whose substitution for Ca^{2+} is used for paleo proxy(ies), based on the partitioning of each between the fluid and aragonite phases (Gaetani et al., 2006; Marchitto et al., 2018; Hathorne et al., 2013; DeCarlo et al., 2015).

DIC = Dissolved Inorganic Carbon; TA = Total Alkalinity. Diagram not to scale. See Table S1 for a list of geochemical proxies analyzed in this study, and their interpretation.

Figure 1. Box 1. Overview of coral calcification and controls on calcifying fluid geochemistry (Furla et al., 2000; Zoccola et al., 2015; Gaetani & Cohen, 2006; Marchitto et al., 2018; Hathorne et al., 2013; DeCarlo et al., 2015; McCulloch et al., 2017; Cohen & McConnaughey, 2003; Al-Horani et al., 2003; Zoccola et al., 2004; Tanaka et al., 2015). Figure 1 modified from Thompson (in review).

Pacific, multi-century synthesis of corals' ability to buffer calcifying fluid chemistry in response to changing ocean conditions, including acidification, warming, and (internal and forced) variability.

Results and Discussion

Seasonal pH, DIC and Ω of coral calcifying fluid

Here we compare new reconstructions of SST and calcifying fluid geochemistry (Table S-1) from modern and subfossil Galápagos corals with published reconstructions from the GBR ((McCulloch et al., 2017; Ross et al., 2017; D'Olivo, Ellwood, et al., 2019)). Two 18^{th} century cores collected at Wolf Island show that as SST increases, pH_{cf} decreases (pH reported on the total scale throughout). The slope of this relationship (WLF04: m = -0.022 pH units per °C, N = 33, r^2 = 0.52; WLF05: m = -0.033 pH units per °C, N = 45, r^2 = 0.43; Figure S1) is nearly identical to that found among replicate modern corals from the GBR (Davies-02: -0.035 pH units per °C, N = 50, r^2 = 0.82; Davies-03: -0.020 pH units per °C, N = 54, r^2 = 0.80). The seasonal pH_{cf} change is also similar among GBR modern and the Wolf fossil coral, with a -0.03 to -0.06 unit change between the average warm and cold seasons (Table S2) and a range of 0.2 to 0.3 pH units at each site. However, the SST-pH relationship weakens in the two modern (20^{th} century) Wolf corals, which display a reduced seasonal pH range (ΔpH = -0.003 to -0.02, Table S2) and a weaker relationship with temperature (i.e., a shallower slope and lower r^2) compared to fossil Wolf cores (Fig. S1).

Comparing modern and fossil data from Wolf, we demonstrate that the pH_{cf}-SST relationship is significantly weaker in the modern corals than in the fossil corals. In contrast, the Wolf fossil and GBR modern corals are not significantly different from one another (Figure 3a). The greater SST range in modern cores (Fig. 3, x-axis) would by itself strengthen this relationship (as in (D'Olivo, Ellwood, et al., 2019)) and therefore cannot explain the observed patterns; we therefore infer that the weakening is likely driven by reduced pH upregulation, due to impacts of OA and/or thermal stress (rather than by temperature-induced changes in calcification or buffering capacity alone (Guo, 2019)). The difference in slope between the fossil and modern corals equates to 7-40% difference in H+ ions in the calcifying fluid (with larger changes at lower temperatures). As a result, Ω_{cf} displays a significant positive relationship with SST in modern Wolf corals, with up to 5% lower saturation during the cold season (September-November; SON) relative to the warm season (Table S2). In contrast, there is no re-

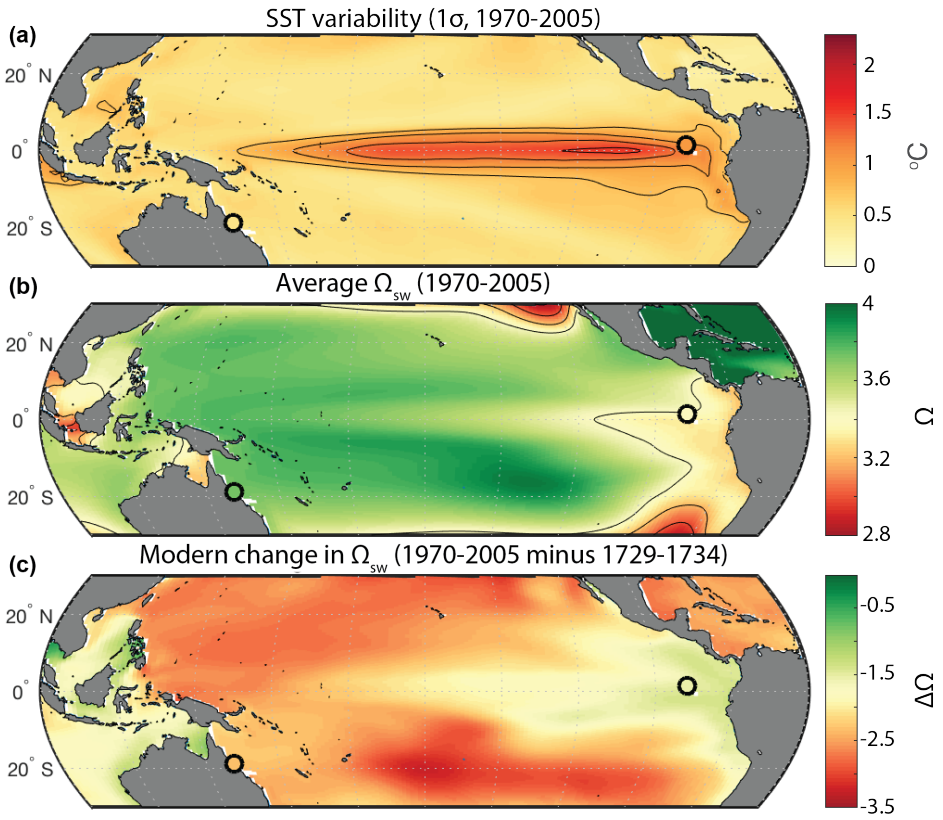

Figure 2. Map of study sites across tropical Pacific Ocean testbed: (a) Interannual variability in sea-surface temperature (SST), calculated from standard deviation of CESM1 LME SST (see Fig. S2 for validation against IGOSS SSTs, (Reynolds et al., 2002)); (b) aragonite saturation state Ω_{sw} at 0m, calculated using CO2SYS (Lewis et al., 1998) from CESM1 LME temperature, salinity, pH_{sw}, and dissolved inorganic carbon (DIC) over the climatological period (1970-2005); and (c) difference in CESM1 LME Ω_{sw} between the modern and 18th century periods studied here. Values for the Great Barrier Reef (Davies Reef) and Galápagos (Wolf Island) study sites are indicated by filled circles; validation of CESM1 against observational values can be found in Table S3.

lationship between Ω_{cf} and temperature in the fossil coral (Fig. 3c) and $< 1.5\%$ change in Ω_{cf} seasonally (Table S2). These results indicate that the fossil corals maintained a steady aragonite saturation state in their calcifying fluid across seasonally varying environmental conditions, while the modern corals did not. Put another way, modern Wolf corals appear to have partially lost their ability to buffer calcifying fluid chemistry against changes in seawater pH and Ω. This result implies a loss of resilience that is likely to lead to reduced calcification under continued environmental change.

Further, the mean and seasonal-interannual variance in calcifying fluid geochemistry were broadly reproducible across cores from both periods (within and among colonies at a single site; Table S2, Figure 4, S1 & S10). However, an anomalously low δ^{11}B and B/Ca departure in core WLF05 co-occurring with a low-density and high Sr/Ca-SST anomaly in 1731-1732 emphasizes the need for further work to assess the impact of skeletal density, microstructure (Chalk et al., 2021), and transect quality (Reed et al., 2019, 2021) on skeletal geochemistry within a single colony. Such within colony variations are likely to be more severe at marginal reef sites like the Galápagos Islands, where corals are susceptible to boring bivalves and display lobate growth structure and complex microscale growth features, such as convergent corallite fans, changes in growth direction, and corallites angled relative to the sampling plane (Reed et al., 2021). Nevertheless, outside this short-lived anomaly, the geochemical relationships reported here were reproducible within replicate cores from a single Galápagos fossil coral colony, with no significant differences in slope between the replicate fossil cores (Fig. S1). The only exception was the relationship between δ^{13}C and DIC_{cf} (Fig. S1c)—suggesting that proxies for metabolic activity may be most susceptible to skeletal microstructures, overall transect quality, symbiont density and composition, and/or shading within colonies with complex 3D structures. Nevertheless, the reproducibility of these relationships suggests that this technique can help expand our knowledge of calcifying fluid geochemistry prior to the industrial era.

Although the absolute magnitude of DIC and Ω upregulation inferred from B/Ca is dependent on the partitioning coefficient (K_D) formulation and the extent of $[Ca^{2+}]$ enrichment in the cf, sensitivity tests demonstrate that the differences in pH and Ω upregulation across sites and time periods are robust regardless of the choice of K_D and $[Ca^{2+}]_{cf}$ (Figures S3-S5). Further, the values are within the range of those obtained through independent micro-sensor measurements (Sevilgen et al.,

2019); recent work comparing δ^{11}B- and microelectrode-based pH_{cf} support the utility of δ^{11}B as a proxy for diurnally-averaged pH_{cf} (Guillermic et al., 2020).

Nevertheless, we note that the controls on pH upregulation and DIC_{cf} likely differ across sites. In Australia, seasonal upregulation of pH_{cf} occurs in response to seasonal variations in temperature (Guo, 2019; D'Olivo, Ellwood, et al., 2019), pH_{sw} (D'Olivo, Ellwood, et al., 2019), and metabolic DIC availability (McCulloch et al., 2017), with lower DIC during the winter months due to reduced light and cooler temperatures (McCulloch et al., 2017). This mechanism was proposed in the GBR and Ningaloo Reef, Australia, where both DIC_{cf} and DIC_{cf}/DIC_{sw} display a strong positive relationship with temperature (McCulloch et al., 2017). This pH seasonality is consistent amongst a wide range of reefs, including the GBR, Coral Sea, Western Australia, Caribbean, and Central Pacific (Knebel et al., 2021; Hemming et al., 1998; Pelejero et al., 2005; McCulloch et al., 2017; D'Olivo & McCulloch, 2017; Ross et al., 2019; D'Olivo, Ellwood, et al., 2019; Chalk et al., 2021). However, all of these sites have fundamentally different dynamics than in the Galápagos, where the cool season experiences upwelling of DIC-rich waters (Kessler, 2006) that impacts the seasonality of CF chemistry. As a result, we find that DIC_{cf} in Wolf corals is independent of temperature in both modern and fossil corals (Fig. 3b). Further, DIC_{cf} is upregulated by a near-constant factor of $\sim$2 relative to DIC_{sw} in modern Wolf corals, compared with a stronger, and seasonally varying DIC_{cf} enrichment in GBR corals (DIC_{cf}/DIC_{sw} = 2.2-3.2, Table S2) and Galápagos fossil corals.

Dissolved Inorganic Carbon & δ^{13}C variability

Comparison of the carbon isotopic (δ^{13}C) variability among cores may explain why pH regulation is weaker in modern Wolf corals (Fig. 3e). First, the relationship between δ^{13}C and the DIC_{cf} in Wolf modern and fossil corals is weak or absent, suggesting that metabolic processes and upwelling contribute approximately equally to the carbon pool at this site. During the cool season, DIC_{cf} is high as a result of both metabolic processes (which preferentially remove light carbon, enriching the carbon pool and increasing skeletal δ^{13}C; as reviewed by (Swart, 1983)) and upwelling (which contributes isotopically light carbon, decreasing skeletal δ^{13}C); therefore the signals compensate, reducing δ^{13}C variance relative to that of DIC_{cf}. Nevertheless, we note a weak negative relationship between δ^{13}C and DIC_{cf} in modern corals (even with the outlier point removed), in addition to consistently more

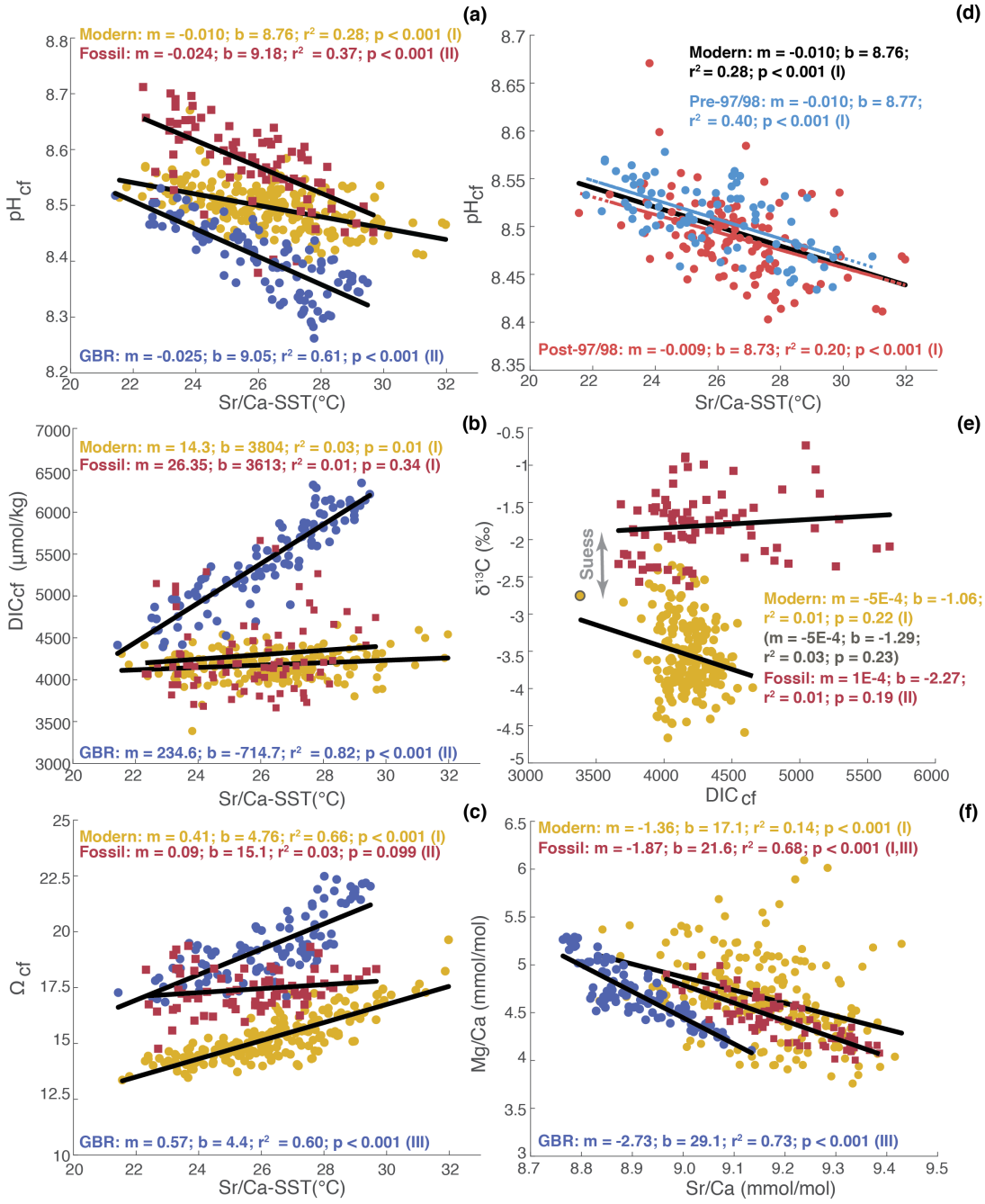

Figure 3. Comparison of the relationships among geochemical proxies (Box 1), Wolf 18th-century fossil (red squares) and modern (20th century, orange circles) versus Great Barrier Reef modern (blue circles): (a) Sr/Ca-SST vs. pH_{cf}, (b) Sr/Ca-SST vs. DIC_{cf}, (c) Sr/Ca-SST vs. Ω_{cf}, (e) DIC_{cf} vs. $\delta^{13}C$ (with and without flier outlined in gray), and (f) Sr/Ca vs. Mg/Ca. Comparison of the pre- 1997/98 thermal stress (blue), and post- 1997/98 thermal stress (red) Sr/Ca-SSTs vs. pH_{cf} for all modern coral data (black) is shown in (d). In all panels, roman numerals (I-III) denote relationships that are significantly different from other groups, based on ANCOVA and multiple comparisons (where a significant difference among groups was identified). Groups with the same roman numeral are not significantly different from one another.

negative $\delta^{13}C$ values in the modern samples from the burning of fossil fuels ("Suess effect"). Although additional data is needed to assess the complex interplay of DIC variability at this site, these results suggest that the upwelling of isotopically light carbon is increasingly dominating the DIC_{cf} pool as the seawater DIC pool becomes isotopically lighter and the coral-algae symbiosis becomes increasingly stressed. Indeed, a significant relationship between $\delta^{13}C$ and DIC_{cf} is only present in the post 97/98 data (Figure S6), driven primarily by large isotopically heavy, low DIC anomalies during and following thermal stress and bleaching.

We also find a notable decrease in DIC_{cf} variability between fossil and modern corals. To assess the strength of DIC upregulation, we use simulated values for seawater carbonate parameters that are unavailable from coral proxies (see Methods), but that compare reasonably well to the limited available direct seawater observations at nearby locations, collected over disparate time periods (Table S3). We find that Galápagos modern DIC_{cf} never reaches above 2.2 times that of DIC_{sw} (DIC_{cf} max = 4654 μmol/kg vs. DIC_{sw} max = 2091 μmol/kg (Manzello, 2010)), whereas the fossil coral DIC_{cf} reaches as much as $\sim$2.8 times that of seawater (5663 μmol/kg, which is within the range observed at the GBR, Fig. 3b). These results are consistent with a larger contribution of metabolic carbon to the DIC pool (values $DIC_{cf}/DIC_{sw} > 1$) in the fossil coral, with large seasonal (Table S2) and interannual variability (Fig. 4e) that reflects the relative strength of upwelling (DIC_{sw}) and photosynthetic carbon fixation (DIC_{cf}) in response to light and temperature. Further, the weak relationship between DIC_{cf} upregulation and Ω_{sw} across all Wolf corals (Table S4) suggests that this decrease in DIC_{cf} variability from pre-industrial conditions is likely driven primarily by dysbiosis (i.e., bleaching or loss of healthy coral microbiome and thus a reduction in metabolic carbon) associated with thermal stress, rather than OA. This is consistent with DIC_{cf}/DIC_{sw} departures of < 1 (i.e., loss of metabolic carbon) during the 1997/98 thermal stress in both modern cores (equating to a 14-34% reduction in DIC upregulation, Fig. 4e). Similar reductions in DIC_{cf} upregulation are observed during other warm extremes in the modern record, whereas DIC upregulation is highest during warm periods in the fossil record. Our results therefore add to the growing body of work identifying adverse effects of thermal stress and bleaching on coral CF chemistry under ocean warming (D'Olivo & McCulloch, 2017; Schoepf et al., 2015, 2021; D'Olivo, Ellwood, et al., 2019; Dishon et al., 2015). The changes in DIC upregulation identified here imply that extreme thermal stress undermines coral health via photosynthetic reductions

that deprive the colony of the energy needed to drive the Ca-ATPase pump and/or other active pathways (e.g., other alkalinity pumps or paracellular transport) that upregulate pH_{cf}, leaving them more susceptible to regional changes in DIC_{sw} and pH_{sw}.

Taken together, these results suggest that DIC_{cf} variability in Wolf corals reflects a complex seasonal interplay between upwelling (cold, high DIC_{sw}, low $\delta^{13}C_{cf}$; May-Nov cold season) and photosynthetic / metabolic (warm, high DIC_{cf}, high $\delta^{13}C_{cf}$; Dec-April warm season) processes, the latter of which contributes less to the carbon pool in modern Wolf corals. Regional upwelling elevates both concentrations and variability of DIC_{sw}; these combine with the coral's metabolic variations to produce fundamentally different DIC_{cf} dynamics at this site (e.g., relative to the GBR). In other words, in Galápagos corals, pH upregulation is partly driven by variations in the seawater carbon pool, rather than changes in metabolic pathways alone. We find that seasonal pH_{cf} variations at Wolf (Table S2) are driven primarily by seasonal temperature and pH_{sw} variability (e.g., 73% and 33%, respectively, in the longest core WLF10-10; after (D'Olivo, Ellwood, et al., 2019); see Methods). These results imply that Galápagos corals are more sensitive to environmental drivers, whereas metabolic processes can regulate cf chemistry more strongly in GBR corals.

Temporal variability in pH_{cf} & impact of thermal stress

Comparing the temporal evolution of pH_{cf} among GBR and Wolf corals over the late 20^{th} century supports our interpretation that corals experience difficulty upregulating pH_{cf} as seawater conditions become less favorable. First, modern Wolf corals display an abrupt drop and subsequent rise in pH_{cf} during and following the 1997/98 El Niño event (Fig. 4a), respectively; this event was characterized by extreme temperature anomalies (Jimenez et al., 2018) (Fig. 4g), stress and bleaching (Glynn, 2001). The decrease in pH_{cf} (towards ambient values) likely resulted from a combination of the loss of metabolic DIC from symbiotic photosynthesis (weakening the ability of corals to regulate their internal pH via the Ca-ATPase or other alkalinity pumps), the regional increase in pH_{sw} (due to reduced upwelling of cold, low pH waters), temperature-induced changes in buffering capacity, and the bleaching-related reduction in calcification rate. The latter is supported by the greater change in pH_{cf} in WLF-3, in which calcification rate declined by 26% in 1998 (Fig. S7). In turn, these changes impact Ω_{cf} regulation (Fig. 3c and S6d), calcification, and thus the imprint of Rayleigh fractionation on the widely

utilized Sr/Ca-SST proxy (with less fractionation following bleaching, suggesting a slowdown in calcification, Fig. S6h). Therefore, although our results are reproducible among proxy-based and observational SST data (Figure S8-9), the breakdown of pH upregulation in modern corals (particularly post-thermal stress and bleaching) may be even greater than indicated by SST proxy records (see Supplemental Text, Figure S8).

The full suite of geochemical tracers measured in modern Galápagos corals provides additional support for the thermal sensitivity of active transport pathways (Ca-ATPase pump, other alkalinity pumps, and/or paracellular transport), particularly following the 1997/98 El Niño event (see supplementary text; Figs. S6 and S10). Departures in U/Ca, Mg/Ca, and $\delta^{13}C$ suggest changes in $[CO_3^{-}]$, Rayleigh fractionation, active transport, and photosynthetic activity following acute thermal stress that are consistent with our interpretations from reconstructed Sr/Ca-SST, DIC_{sw}, and pH (see supplemental text). For example, the relationship between Sr/Ca and both Mg/Ca and U/Ca weakens significantly after 1997/98, implying weaker Rayleigh fractionation and/or reduced active transport. A weakening of the pH-SST relationship after 1997/98 (Figs. 3d and S6a) also supports the hypothesis that corals lose their ability to regulate pH_{cf} via the Ca-ATPase pump or other active pathways post-stress. However, our results are based on relatively few data following this stress event, limiting the significance of these changes (Figs. S6a); similar analyses of additional stress events would clarify these patterns and improve interpretations of calcification and skeletal geochemistry following thermal stress and bleaching. Nevertheless, these results are consistent with other recent studies demonstrating acute impacts of thermal stress on pH_{cf} and skeletal geochemistry (McCulloch et al., 2017; Ross et al., 2017; D'Olivo & McCulloch, 2017; D'Olivo, Ellwood, et al., 2019; Guillermic et al., 2020; Clarke et al., 2017, 2019; Schoepf et al., 2021).

Upregulation of pH, DIC, and Ω

To understand how corals will respond to ongoing and future environmental changes, it is critical to assess the capacity of corals to regulate Ω_{cf} across sites and time periods with different baseline seawater chemistry. Here, we demonstrate that despite large changes in seawater chemistry between the 18^{th} century and modern periods inferred from model simulations (Fig. 2c), there is no relationship between Ω_{sw} and the upregulation of Ω_{cf} in Galápagos corals (Table S4). In other words,

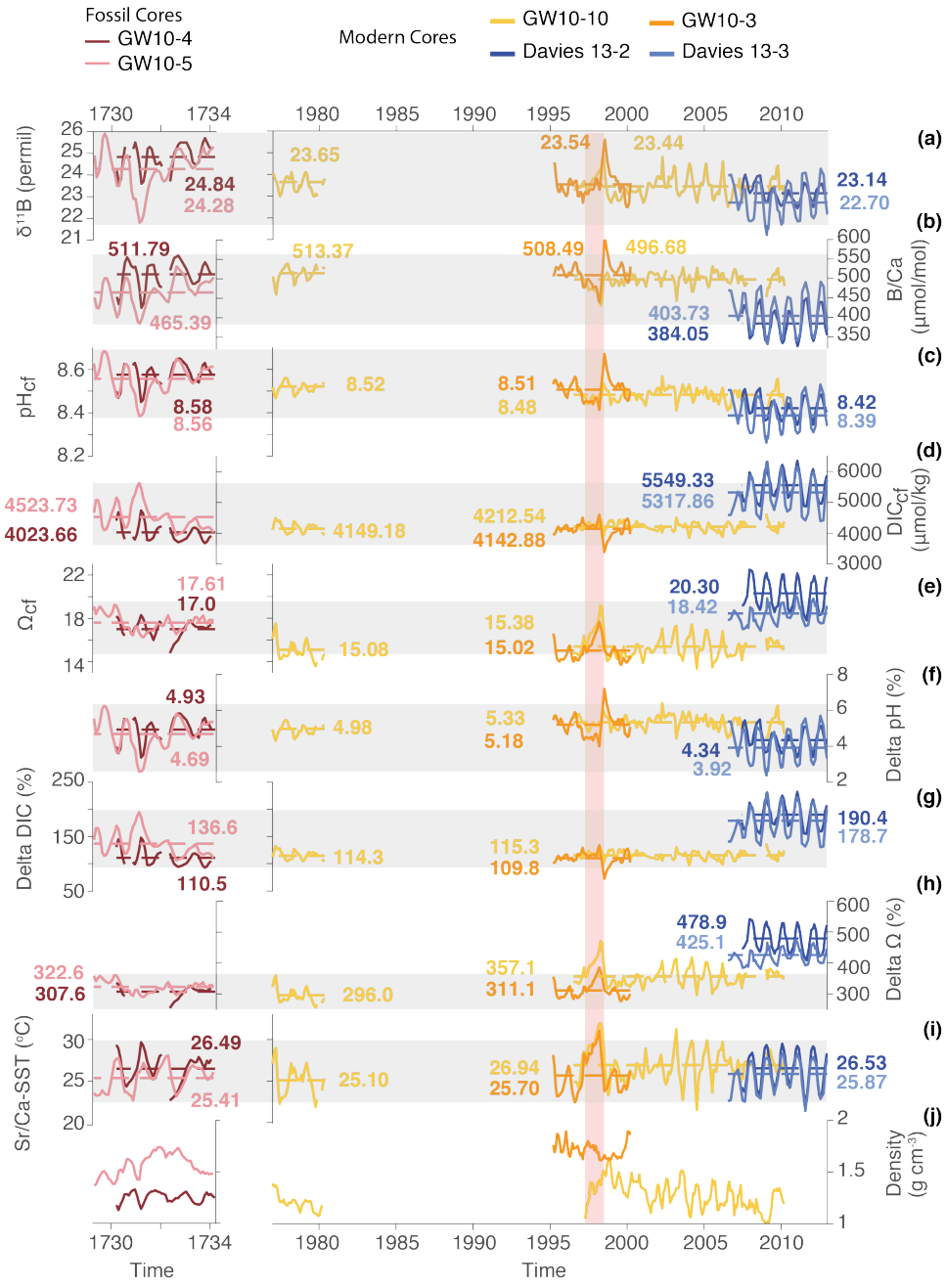

Figure 4. Time series of boron-derived calcifying fluid geochemistry, Sr/Ca-SSTs, and skeletal density: Wolf 18th-century fossil (red) and modern (20th century, orange) versus Great Barrier Reef (blue). (a) δ^{11}B (permil), (b) B/Ca (μmol/mol), (c) pH_{cf} (total scale), (d) DIC_{cf} (μmol/kg), (e) Ω_{cf}, (f) Percent upregulation of pH_{cf} with respect to pH_{sw} (%), (g) Percent upregulation of DIC_{cf} with respect to DIC_{sw} (%), (h) Percent upregulation of Ω_{cf} with respect to Ω_{sw} (%), (i) Sr/Ca-SSTs (°C), and (j) skeletal density (g/cm^3). See Methods for how these parameters were derived from proxy and model data. Gray shading depicts the range of 18th-century fossil values; red shading depicts warm anomalies associated with the 1997/98 El Niño event; mean values are denoted by dotted lines on each series.

304 Ω_{sw} has not had a detectable influence on upregulation capacity, implying that Galápagos corals have
305 not adapted their capacity to regulate Ω_{cf} in response to thermal extremes and OA since the pre-industrial
306 era. Therefore, although they continue to regulate their internal growth environment at maximum ca-
307 pacity, the resulting calcifying fluid saturation levels in are significantly lower in modern corals due
308 to OA.

309 Our results contrast with the apparent pH "homeostasis" observed in extreme environments (near
310 submarine seeps in Papua New Guinea (Wall et al., 2016) and Puerto Morelos, Mexico (Wall et al.,
311 2019)) and in the Heron Island (GBR) FOCE (Georgiou et al., 2015). At these pCO_2 extremes, *Porites*
312 spp. corals show a strong relationship between Ω_{cf} upregulation and seawater conditions (e.g., $\Delta\Omega_{cf}$
313 of 214% and 270% per unit change in Ω_{sw}, respectively, Table S4). However, in both scenarios, Ω_{sw}
314 was 19-82% lower than observed on any modern reefs studied here. Further, seep corals have persisted
315 in these conditions for multiple generations and likely have acclimatized and/or adapted to low sea-
316 water saturation over long time periods. Therefore, such sites are unlikely to be good analogues for
317 adaptation potential to current rates of OA, which can occur over the lifetime of an individual coral
318 (100+ years). Therefore, despite the potential for acclimation indicated by such studies of extreme
319 conditions, under the real-world environmental change and multivariate stresses, Galápagos *Porites*
320 spp. corals have not demonstrated an ability to adapt to changing pH via pH_{cf} upregulation.

321 Our synthesis of modern and fossil corals living under contrasting seawater conditions suggests
322 that there may be a physiological limit to the capacity of corals to upregulate pH_{cf} in response to chang-
323 ing ocean condition and fluctuations in DIC_{cf}. The capacity of corals to upregulate Ω_{cf} is therefore
324 likely to be dictated (to the first order) by their capacity to upregulate DIC_{cf}, which we show is re-
325 duced both at marginal sites and following bleaching. Galápagos corals, which have low DIC_{cf} *despite*
326 high regional DIC_{sw}, therefore require greater pH_{cf} upregulation than modern GBR *Porites* spp. corals
327 to maintain similar rates of calcification. Such a physiological limit, if it holds across future acidifi-
328 cation (and across additional sites), is likely to leave corals in low-pH, high-DIC environments (i.e.,
329 in marginal environments) particularly susceptible to changing ocean saturation.

330 At both sites, the degree of pH_{cf}, DIC_{cf}, and Ω_{cf} upregulation relative to seawater varied in con-
331 cert with SST; warm seasons or years experience greater Ω_{cf} and DIC_{cf} upregulation, and weaker pH_{cf}
332 upregulation (Table S2 & S5; Fig. 4d-g). These results agree with previous work showing a strong re-

lationship between pH_{cf} upregulation and temperature across a latitudinal gradient (Ross et al., 2019). Physicochemical modeling of coral cf chemistry suggests the temperature dependence of pH upregulation is driven primarily by calcification kinetics, and secondarily by seawater buffering capacity (i.e., the sensitivity of the pH_{cf} to changes in total alkalinity) (Guo, 2019). This dependence is particularly apparent during the 1997/98 El Niño in Wolf modern corals, with anomalously high pH_{cf} and high Ω_{cf} relative to seawater during and immediately following peak warming (January 1998 to September 1998), potentially due to increased buffering capacity at higher temperatures. However, the increase in pH_{cf} upregulation following peak warming (i.e., during the stress recovery period) implies that other physiological mechanisms must also be at play, such as a change in the refresh rate of the cf or a change in the balance of bicarbonate and carbonate that is transported to the site of calcification (D'Olivo & McCulloch, 2017). Although uncertainties in the fidelity of the Sr/Ca-SST proxy across this thermal stress event may add uncertainty to the SST signal (D'Olivo & McCulloch, 2017), only ∼2% of the pH_{cf} anomaly can be explained by SST alone, and the Ω upregulation anomaly (i.e., 97/98 $\Delta\Omega$ relative to the colony mean $\Delta\Omega$, Fig. 4h) is robust between the replicate modern cores (23 and 31%) despite differences in calcification rate between colonies. Nevertheless, similar Ω upregulation anomalies does not preclude differences in the relative roles of DIC_{cf} and pH_{cf} in this saturation change (Fig. 4). Our results suggest that although the response of metabolic carbon production and/or pH_{cf} to thermal stress varies from colony to colony, the relative change in Ω_{cf} with respect to seawater does not vary significantly among colonies. Again, these results demonstrate strong physiological limits to the corals' ability to regulate their internal carbonate chemistry, and that this limit is likely an emergent property resulting from the interplay of numerous physiological processes or pathways.

Implications for calcification under warming & acidification

Our results demonstrate that physiological limitations have already had a pronounced impact on the geochemistry of the calcifying fluid in Galápagos *Porites* sp. corals. The pH_{cf} declined significantly between 18th century and modern Wolf corals ($Z = 24.3$, $N = 108{,}277$, $p < 0.001$), and from 1975 to 2010 in the long modern Wolf (GW10-10) record (with a trend of -0.18 pH units per decade). Over 99.9% of this recent trend (between 1975 and 2010) can be attributed to pH_{sw}, with warming contributing less than 0.3% (after (D'Olivo, Ellwood, et al., 2019); see methods). The mean pH_{cf} was

8.57 in two 18th century fossil cores from one colony (N = 78) and 8.50 in the two modern corals (N = 203, Fig. 4, Table 1). This pre-industrial to modern mean pH_{cf} difference can be attributed some combination of pH_{sw} or SST changes. A large model ensemble of simulated changes between these periods suggests that either pH_{sw} or SST could produce pH_{cf} changes of 0.06-0.07 (see methods). In contrast, the temporal change in DIC_{cf} differs between cores, consistent with a varying role of photosynthesis (and thus metabolic carbon) among (and even within) colonies. The combined impact on saturation state was profound, with a significant decline of ∼2.3 units between the 18th century and late-20th century corals ($Z = 24.2$, $N_{fossil} = 108$, $N_{modern} = 277$, $p < 0.001$). These results emphasize the importance of extending the existing boron reconstructions across time periods that experienced different seawater chemistry from today. This initial study focused on replicate cores from one colony, and it will be critical to further replicate and extend these analyses to other fossil colonies to confirm these findings (given the potential for within and among colony differences in boron geochemistry, e.g., (Chalk et al., 2021)). Nevertheless, the first such application of boron systematics to pre-industrial fossil coral samples, presented here, paints a potentially stark future under projected acidification, suggesting limited adaptive capacity in the upregulation of the coral calcifying fluid.

Despite this reduction in pH_{cf} between the 18th and 20th century Galápagos corals, there was no significant change in calcification or skeletal density among cores (or between modern and fossil colonies; see section "Coral densitometry and calcification" for description of methods). This is in contrast to previous work that demonstrates a strong relationship between calcification and pH_{cf} (Ross et al., 2019; Guillermic et al., 2020), and suggests that the impact of warming on calcification kenetics may at least partially compensate (albeit with the added risk of thermal stress and bleaching). Rather, we find large interannual changes in calcification rate within (15-27%) and among (24-27%) cores (Table S6; Fig S7). The predicted change in calcification between the 18th and 20th centuries (-10%, using predicted Ω_{sw} from Fig. 2c, the Ω_{cf} Pchange from Table S4, and the model of (McCulloch et al., 2012), see methods) therefore falls within the range of interannual calcification variability at this site. Thus, despite large declines in Ω_{cf}, the impact on coral calcification is not yet detectable at Wolf Island, Galápagos given the high interannual calcification variability.

However, these results should not be interpreted as evidence that Galápagos corals are robust to changing ocean chemistry, for five reasons. First, monthly skeletal density data is strongly related

to both CF saturation state and temperature in both fossil and modern Galápagos corals (Fig. 4). Although the nature of these relationships vary across cores (see Table S7; e.g., as a function of colony-to-colony variations in bleaching susceptibility), the relationships indicate declining density with warming and lower cf saturation (except in core WLF-3) and an increasing importance of warming in recent decades (becoming the dominant predictor in core WLF-10a, ending in 2010). Second, the corals studied here are likely to represent the "best-case-scenario", as these long-lived corals targeted for paleoclimate reconstructions are the "winners" that were able to maintain rapid upward extension and calcification despite thermal stress (1997/98) and acidification (Fig. S7). In smaller *P. lobata* colonies at nearby Darwin Island (Manzello et al., 2014), calcification rates were less than half those measured in our longer Wolf cores, despite similar density values among colonies from both sites (Table S6). Further, the modern Wolf colonies regrew in 3.4 (WLF10-10) and 5 (WLF10-03) years following the very strong 1982/83 El Niño event that devastated reefs across the Galápagos (Glynn et al., 1988), suggesting they experienced only partial mortality during this extreme event. Both colonies also displayed only modest reductions in extension and calcification during or following the 1997/98 event (Figure S7). Because paleoclimate records are biased towards corals that survive, they likely yield a conservative (i.e., too-stable) estimate of past calcification change(s). Third, observed and simulated ocean pH at Galápagos remained above 8.0 over this period (mean CESM1 = 8.08-8.11 over intervals of coral coverage; Darwin = 8.07 (Humphreys et al., 2018)), a critical tipping point below which corals across the archipelago suffer reduced calcification and structural persistence (Manzello et al., 2014). High nutrients (Manzello et al., 2014) and variable seawater conditions exacerbate the stressful impacts of acidification in upwelling regions, resulting in tipping points at higher pH values (Manzello et al., 2014). Fourth, the temperature dependence of calcification kinetics does not appear to compensate for the impacts of saturation-state changes at Wolf (unlike in more optimal environments; (Burton & Walter, 1987; Lough & Barnes, 2000)). Lastly, and critically, we demonstrate that as oceans acidify, Wolf corals have not intensified their upregulation of pH or Ω.

Finally, our results support the potential to reconstruct changes in paleo-pH from the geochemistry of coral calcifying fluid. Consistent with recent studies (Guo, 2019; D'Olivo, Ellwood, et al., 2019), the narrow range in pH_{cf} upregulation of *Porites* spp. across sites and time periods (Table S4) suggests that within this paleo-relevant genus, long-term pH_{cf} trends are primarily driven by pH_{sw} and

not physiological controls (which regulate calcifying fluid chemistry on seasonal timescales, in response to temperature-related changes in DIC, calcification and buffering capacity). Physiological limits in this capacity to regulate pH_{cf}—identified here for the first time—suggest that as seawater saturation shifts to lower values (as observed with ocean acidification, or across spatial gradients (Manzello et al., 2014)), so will the distribution of carbonate saturation in the calcifying fluid (as observed between 18^{th} and 20^{th} corals). Corals' capacity to buffer against ocean acidification may therefore be more limited than predicted from experimental manipulations and extreme environments (CO_2 seeps), with particularly severe consequences for corals at marginal sites characterized by reduced metabolic carbon production, low seawater pH, and frequent or severe stress.

Methods

Coral Core Collection

We collected cores from modern (living) and underwater sub-fossil (i.e., deceased upon collection; hereafter "fossil") *Porites lobata* colonies in Shark Bay, along the northeastern shore of Wolf Island, Galápagos (1^o23.15'N, 91^o49.90'W) in May-June 2010. Here, we analyze four cores from three colonies (two modern, and one fossil): (1) GW10-3 (modern), collected from 10m depth; (2) GW10-10 (modern), collected from 12m depth; and (3) GW10-4 and (4) GW10-5 collected from the same fossil colony at 13m depth. We compare these geochemical records from Wolf to published data from Davies Reef, Great Barrier Reef (cores 13-2 and 13-3 (McCulloch et al., 2017)).

Sub-sampling & Age Determination

All cores were milled at continuous 2 millimeter increments for geochemical analysis; based on average modern extension rates (GW10-3 = 12.4 mm/year, GW10-10 = 20.3 mm/year), this sampling increment resolves sub-seasonal (bimonthly or better) variability of coral skeletal geochemistry and inferred environmental parameters. This resolution was selected based on the time- and sample-intensive nature of the ion exchange chromatography required for boron isotopic analysis; given these constraints, this work presents a significantly extends the network of long, high-resolution, multi-proxy data. Modern corals were re-sampled adjacent to the original sampling transects (Jimenez et al., 2018) across intervals of known climatic extremes (e.g., large eastern Pacific El Niño events) and phases of Pacific

decadal variability, while fossil cores were sampled prior to and following the depths sampled for U/Th age dating (to maximize precision of replicating and splicing these floating chronologies).

Pre-industrial Wolf fossil cores (WLF10-04 and WLF10-5) were U/Th dated at the University of Minnesota following the procedures of (Cheng et al., 2013; Edwards et al., 1987; Shen et al., 2002). Large samples along the same individual annual bands were cut using a Dremel tool from slab D (622 mm from core top; 827 mg) and slab E (46 mm from top of slab E; 869 mg) of cores WLF10-04 and WLF10-5, respectively. These bands were selected from a pristine portion of each core, aiming to obtain overlapping, replicate dates for this colony (using the estimated offset between core tops and band counting). U/Th samples were cleaned thoroughly with DI water, first with a water pick and then with repeated ultrasonic agitation (until loose powder no longer collected in the basin); finally, samples were dried overnight at 30^{o}C. Ages were corrected for initial, non-radiogenic Th using an initial $^{230}Th/^{232}Th$ atomic ratio of 4.4 ± 2.2E-6. This is the expected value for a material at secular equilibrium, with a bulk earth $^{230}Th/^{232}Th$ of 3.8. Errors were conservatively assumed to be ± 50%. Wolf10-04 and WLF10-05 sample ages were 1732 ± 7 and 1738 ± 5 C.E., respectively (see (Reed et al., 2021) for full U/Th results).

These floating chronologies were tied to the complete Sr/Ca record from WLF10-4 (Reed et al., 2021) to optimize correlation among the series within the uncertainty of the U/Th dates. However, all Wolf fossil coral series are floating chronologies (i.e., they are not tied to overlapping modern records); thus, we estimate an absolute age error as ±5-7 years (based on the precision of the U/Th dates). Therefore, we restrict trend analysis to absolute differences between the modern and pre-industrial periods, rather than on rates of change.

Age-depth models for all cores were developed using linear interpolation in MATLAB between seasonal Sr/Ca-SST tie points. Due to high interannual variability in the timing of the cool season minima (during winter) the age model relies only on summer tie points. Sr/Ca minima were tied to March SST maxima; tie points for modern Wolf cores (WLF10-3 and WLF10-10) are identical to those published in (Jimenez et al., 2018). Data were linearly interpolated to obtain monthly records for time-series analysis. Although this approach may introduce sub-annual chronological errors, regressions among geochemical proxies that form the core of this study were performed on the raw data (prior to age modeling) and are not influenced by chronological errors or interpolation. Finally, we used Sr/Ca-SST re-

constructions from GW10-3 (2010-1987; 1983-1940) and GW10-10 (2010-1985; 1982-1975) published by (Jimenez et al., 2018) for comparison.

Trace Elemental Geochemistry

All trace elemental analyses were performed on a Quadrupole-ICP-MS (X-series II Q-ICP-MS, Thermo Fisher Scientific) at the University of Western Australia. First, sub-samples of 10 ± 0.2 mg of coral powder were weighed, dissolved in 500 μL of 0.51N HNO_3, agitated, and centrifuged for 1 minute at 3500rpm. A 38 μL aliquot of dissolved powder was diluted in 3 mL of 2% HNO_3 (100 ppm Ca) for trace elemental analysis; the remaining 400 μL of the dissolved powder was used for boron isotope analysis (see below). Analysis of ^{7}Li,^{25}Mg, and ^{11}B by Q-ICP-MS was performed on the 100 ppm Ca dilution, while an additional 300 μL sub-aliquot of the 100 ppm Ca solution was diluted (to 10 ppm Ca) in 2.7 mL of a 2% HNO_3 spike solution (containing ∼19 ppb ^{45}Sc, 19 ppb ^{89}Y, 0.19 ppb ^{141}Pr, and 0.095 ppb ^{209}Bi) for analysis of ^{25}Mg, ^{43}Ca, ^{86}Sr, and ^{238}U. Reproducibility for the JCP-1 interlaboratory standard (2σ relative standard deviation, RSD; n = 19) was ± 0.830% for Mg/Ca, ± 0.636% for Sr/Ca, ± 1.341% for U/Ca, ± 3.649% for Li/Mg (N = 17), and ± 3.651% for B/Mg (N = 17).

We used published TE/Ca-SST calibrations to reconstruct SST from the (local) Sr/Ca-SST (McCulloch et al., 2017; Jimenez et al., 2018) and Li/Mg-SST (Montagna et al., 2014) relationships. For Wolf corals, we applied the Sr/Ca-SST calibration (m = -0.057 ± 0.001; b = 10.658 ± 0.025) from weighted least squares (WLS) regression of the WLF10-03 and WLF10-10 composite record against OISST between May 1987-March 2010 (Jimenez et al., 2018). The composite calibration was utilized to standardize the calibrations across cores; however, the same results were found when using core-specific calibrations for the modern corals, as the calibration equations were similar between cores (Jimenez et al., 2018). For the Davies Reef, GBR corals, we used the Sr/Ca-SST calibration (m = -0.046; b = 10.12) obtained from local calibration with in-situ temperature data (McCulloch et al., 2017). For both sites, the Li/Mg-SSTs were calculated using the calibration curve of (Montagna et al., 2014). All new trace elemental geochemical data is shown in Figs. 4, S9-S10.

Determination of calcifying fluid pH and carbonate chemistry from boron systematics

The boron in the remaining 400 μL aliquot of dissolved powder (after trace elemental analysis, above) was purified by ion exchange chromatography (after (McCulloch et al., 2014)), and the δ^{11}B was measured by MC-ICP-MS using a NU Plasma II at the University of Western Australia. The measured isotopic ratio of ^{11}B and ^{10}B of the carbonate samples were expressed relative to that of the NIST SRM 951 boric acid standard, in standard delta notation (in units of per mil or ‰):

$$\delta^{11}B_{carb} = \left[\frac{^{11}\mathrm{B}/^{10}\mathrm{B}}{^{11}\mathrm{B}/^{10}\mathrm{B}_{standard}}\right] \times 1000. \quad (1)$$

Reproducibility for the JCP-1 interlaboratory standard (2σ; n = 29) was ± 0.22 ‰.

We used paired boron isotope and B/Ca ratios to determine the pH and carbonate ion concentration, leveraging three key features of boron isotope systematics. First, boron speciation in seawater depends strongly on pH, with borate ion ($B(OH)_4^-$) dominating at higher pH and boric acid ($B(OH)_3$) dominating at lower pH ($< \sim$8.5). Second, boron isotopes are strongly fractionated between the two species, with a +27‰ offset between borate and boric acid. Taken together, as pH decreases, the fraction of boron as borate decreases and the δ^{11}B increases. Third, as corals calcify from a semi-isolated calcifying fluid, borate may substitute for the carbonate ion (CO_3^{2-}) (Sen et al., 1994). Although there are multiple pathways by which this could occur, recent inorganic precipitation studies (Holcomb et al., 2016) suggest that it likely occurs via de-protonation and co-precipitation with CO_3^{2-} ((Noireaux et al., 2015), rather than via bicarbonate or some mixture of the two, as previously proposed (Allison et al., 2014)).

The initial calcifying fluid δ^{11}B and total boron concentrations are thought to the same as that of seawater, as seawater serves as the source of boron; further, the boron isotopic composition and concentration remains relatively constant during calcification, due to low partitioning coefficient (K_D) of B/Ca between aragonite and seawater (i.e., B is strongly excluded from the skeleton during precipitation) (Holcomb et al., 2016). We note that diffusion may violate these assumptions under certain conditions; for example, diffusion of isotopically distinct boric acid may alter the δ^{11}B relative to seawater (Gagnon et al., 2021) or increase boron concentrations relative to seawater when pH is elevated.

However, there is no experimental evidence for these confounding factors within tropical, symbiont-bearing coral species; as symbionts provide an additional critical source of DIC to the calcifying fluid, biomineralization processes in symbiont-bearing corals are markedly different from that of the cold-water species for which these limitations have been identified. We therefore follow the approach of other recently published studies in this regard (Chalk et al., 2021; DeCarlo et al., 2018; D'Olivo, Ellwood, et al., 2019; Ross et al., 2019, 2017; McCulloch et al., 2017).

As a result of these processes, the skeletal δ^{11}B reflects the pH of the calcifying fluid (pH_{cf}), while the [B] reflects both pH and the [CO_3^{2-}] (Holcomb et al., 2016; DeCarlo et al., 2018). We calculate pH_{cf} from δ^{11}B of the carbonate skeleton (after (Zeebe & Wolf-Gladrow, 2001)):

$$pH_{cf} = pK_B - \log\left[\frac{(\delta^{11}B_{sw} - \delta^{11}B_{carb})}{(\alpha_{(B3-B4)}\delta^{11}B_{carb} - \delta^{11}B_{sw} + 1000(\alpha_{(B3-B4)} - 1))}\right], \tag{2}$$

where the δ^{11}B of seawater ($\delta^{11}B_{sw}$) was defined as 39.61‰ (Foster et al., 2010), the boron isotope equilibrium constant ($\alpha_{(B3\text{-}B4)}$) was set to 1.0272 (Klochko et al., 2006), and the dissociation constant of boric acid (pK_B) was calculated from temperature, salinity and pressure (after (Dickson, 1990)). To standardize methods across cores (as *in situ* data is not available for all sites or time periods), we used Li/Mg-derived SSTs and SODA sea-surface salinity (SSS). We used mean climatological SODA SSS (33.5 PSU) for fossil analyses (prior to the industrial era).

Empirical constraints on the B/Ca partitioning coefficient between aragonite and seawater and its dependency on pH_{cf} (Holcomb et al., 2016) permit reconstruction of carbonate ion concentration in the calcifying fluid from paired δ^{11}B-pH_{cf} and B/Ca measurements (DeCarlo et al., 2018):

$$K_D \equiv (\mathrm{B/Ca})_{\mathrm{CaCO_3}} \times \frac{[\mathrm{CO_3^{2-}}]_{\mathrm{cf}}}{[\mathrm{B(OH)_4^-}]_{\mathrm{cf}}}, \tag{3a}$$

$$K_D = 0.00297 \exp(-0.0202[\mathrm{H^+}]_{cf}), \tag{3b}$$

and

$$\left[\mathrm{CO_3^{2-}}\right]_{cf} = \frac{K_D \times \left[\mathrm{B(OH)_4^-}\right]_{cf}}{(\mathrm{B/Ca}_{\mathrm{CaCO_3}})}, \tag{4}$$

where Eq. 3b follows the formulation of (McCulloch et al., 2017). Although there continues to be debate over the best K_D formulation (DeCarlo et al., 2018), Eq. 3b is likely to be most accurate for tropical reef-building corals as it does not include the (Mavromatis et al., 2015) experimental data, which was collected from NaCl solutions (rather than seawater) at very low $[CO_3^{2-}]$ relative to that of coral CF.

As reviewed by (DeCarlo et al., 2018), uncertainties still remain with regards to the most accurate formulation for K_D and the degree to which Ca^{2+} is upregulated within the cf. We evaluated the sensitivity of our results (see Figure S6-7, S10, S14) to the K_D formulation, following the equations of (Holcomb et al., 2016; McCulloch et al., 2017; DeCarlo et al., 2018) and the boron systematics package of (DeCarlo et al., 2018), as well as using a constant K_D of 0.002 (after (Allison, 2017)). Our sensitivity tests show that these uncertainties only marginally impact the absolute magnitude of inferred DIC_{cf} and do not influence the relative changes across sites and time periods (the focus of this work). Further, the inferred DIC_{cf} upregulation is higher using the K_D formulation of (McCulloch et al., 2017) (Figure S6); therefore, our chosen approach produces the most conservative change in DIC_{cf} and Ω_{cf} under warming and acidification. We similarly test the impact of Ca^{2+} upregulation relative to seawater on resulting Ω_{cf} calculations. For this, we use the mean and +/- 1 standard deviation from these independent micro-sensor measurements of ((Sevilgen et al., 2019), Table 1). These sensitivity analyses demonstrate that uncertainties Ca^{2+} impact the absolute magnitude of Ω_{cf} within colonies (Figure S8), but not the relative differences among colonies, sites, or time periods (the focus of this study). We therefore utilize the most conservative approach, and report results using a Ca^{2+} scaling factor of 1, which is the lower (-1σ) bound from from (Sevilgen et al., 2019). Inferred trends in Ω_{cf} and calcification would be greater if a constant K_D or higher Ca^{2+} are assumed (Figure S14). Therefore, the results reported here are the most conservative estimate of inferred Ω and calcification changes from preindustrial to modern conditions.

DIC_{cf} is calculated from the pH_{cf} (Eq. 2) and $[CO_3^{2-}]_{cf}$ using CO2SYS software (Lewis et al., 1998) and the following constants: carbonate species dissociation from (Dickson & Millero, 1987; Mehrbach et al., 1973), borate and sulfate dissociation (Dickson, 1990), and aragonite solubility (Mucci, 1983). Finally, we explore the relationship between pH, DIC and Ω of the coral calcifying fluid and Sr/Ca-SST (note: we utilize Sr/Ca-SST as a quasi-independent SST estimate rather than Li/Mg-SST, as the

latter was used in Eq. 2). Our findings are robust to the paleo-thermometer used to assess the impact of temperature on coral carbonate chemistry (e.g., Fig. S8; see supplemental information).

Stable Isotope Geochemistry

Stable oxygen and carbon isotope ratios (δ^{18}O and δ^{13}C) were analyzed on a Thermo Delta V Plus mass spectrometer, coupled to a Kiel IV carbonate preparation system in the PACE lab, at the University of Michigan' Earth and Environmental Sciences department. Analyses were performed on splits of the same powders analyzed for TE chemistry and paired δ^{11}B-B/Ca boron systematics. Long-term analytical precision (1 sd) of Luxor internal carbonate standard was 0.08‰ for δ^{18}O and 0.05‰ for δ^{13}C. All new stable isotope data are shown in Figs. 4 and S10.

Statistical analysis

Ordinary least squares regressions (OLS) were used to assess relationships among geochemical parameters within and among coral colonies, and in upregulation with respect to seawater conditions. First, OLS regressions were performed among reconstructed calcifying fluid and skeletal geochemical parameters (Figs. 3, S1, S3-S6). ANCOVA and multiple comparisons were then utilized to assess differences in the relationship among groups (i.e., among individual cores, or among fossil Wolf, modern Wolf, and GBR corals). Finally, OLS was utilized to assess the relationship between average upregulation of pH_{cf}, DIC_{cf}, and Ω_{cf} and seawater chemistry and temperature. Confidence intervals (95% CI) were determined from the 5^{th} and 95^{th} percentiles of 1000 random draws of the distribution of upregulation estimates (based on the standard deviation and mean of each record).

Coral densitometry and calcification

Skeletal density was measured using a quantitative X-ray scanning method developed at the Australian Institute of Marine Science ((Anderson et al., 2017) supplementary methods) alongside six compressed *Porites* sp. powder standards. These standards were used to calibrate X-ray grayscale values to known density, by applying a linear fit between known density (multiplied by thickness) and the natural log of each standard's mean grayscale value. Grayscale values were measured from the background-corrected X-ray positives using Fiji software. Analytical precision of these X-ray density measurements

was estimated using an additional standard with a known density (2.3977 g cm^{-2}) and thickness (6.86 mm) with values within the typical range of massive *Porites* spp. coral slabs. The average density of this quality control standard across all five X-rays used in this study was 2.3655 g cm^{-2}; thus, we report an uncertainty of 0.043 g cm^{-2} or 1.8%.

For each core, grayscale values were measured along 4 mm-wide transects on either side of the geochemical transect. We report density values from each transect, as well as the average across both transects (to account for micro-scale variations in density associated with skeletal architecture). For each transect, density was calculated using the standard calibration curve, normalized by slab thickness. Thickness was measured at 0.125 cm increments along two transects, and the average thickness was interpolated to 0.005 cm (the sampling resolution of the X-ray density measurements).

Annual growth metrics (density, extension, and calcification) were calculated from warm season to warm season using annual tie points (Sr/Ca minima, SST maxima). This approach was utilized as the seasonal cycle was more clearly identifiable in the Sr/Ca series (relative to that of the growth series). Extension was calculated as the distance between successive Sr/Ca minima, and calcification as the product of extension and annual average skeletal density.

Seawater Carbonate System

Seawater carbonate chemistry (TCO_2, Total Alkalinity [TA], pCO_2, pH, and Ω_{arag}) were obtained from (Manzello, 2010; Manzello et al., 2014; Humphreys et al., 2018). Briefly, seawater samples were collected during the cool (n = 24) and warm (n = 21) seasons over multiple years in 500 mL borosilicate glass bottles from 7 study sites throughout the archipelago: (1) Bartolomé, Santiago Island; (2) Santa Fe Island; (3) Punta Bassa, San Cristóbal Island; (4) Punta Pitt, San Cristóbal Island; (5) Devil's Crown, Floreana Island; (6) Gardner Bay, Española Island; and (7) Darwin Island (N=7; summary statistics obtained from (Humphreys et al., 2018)). Here, we utilize the mean (± standard error of the mean, SEM) values to assess the relationship between pH_{cf} and DIC_{cf} (calculated from paired coral $\delta^{11}B$ and B/Ca) and regional changes in the seawater CO_2 system. However, available measurements are discrete, disjointed snapshots, and therefore lack temporal information with which to identify variability on interannual and longer timescales. Further, it is important to note that Ω_{arag} at Wolf Island is expected to display higher mean values and lower seasonal variability (see Fig. 1 of (Manzello,

2009)) than the seawater collection sites of (Manzello, 2010), as upwelling and equatorial undercurrent (EUC) strength and variability is weaker at Wolf Island. As values from Wolf Island are not publicly available, analyses were performed using both the in situ data from Darwin Island (Manzello et al., 2014; Humphreys et al., 2018) and Community Earth System Model version 1 (CESM1).

Community Earth System Model Biogeochemistry

Given the sparse network of seawater inorganic carbon measurements (i.e., DIC, pH, alkalinity) with which to calculate seawater aragonite saturation state, we use the CESM1 Last Millennium Ensemble (LME, (Otto-Bliesner et al., 2016)) and Large Ensemble (LE, (Kay et al., 2015)) to compare the chemistry of the coral calcifying fluid to that of local seawater. This approach facilitates comparison across sites, as well as among 18^{th} century (LME), 20^{th} century (LME and LE), and end of 21^{st} century (LE) conditions. The CESM1 marine ecosystem-biogeochemical module (Hurrell et al., 2013) permits analysis of the entire carbonate systems across space and time, permitting the first multi-site, multi-century synthesis of coral calcifying fluid chemistry in response to changing ocean conditions.

The CESM1 LME simulation was validated against OISST SSTs ((Reynolds et al., 2007), Fig. S2), Simple Ocean Data Assimulation (SODA) SSS (Carton & Giese, 2008) (not shown), buoy data (Sutton et al., 2019), seawater samples described above (Table S3), and the spatially interpolated climatology (1972-2013) from GLODAP version 2 (Lauvset et al., 2016) (Table S3). CESM1 simulated pH and calculated Ω_{sw} compare well with the observations across the tropical Pacific, with differences of less than 0.05 and < 0.5 (RSDs of < 0.6 and 8%), respectively (Table S3). Further, these discrepancies may be at least partially attributed to the comparison of discrete in-situ snapshots of ocean pH with the climatological value over different baseline periods (over which there is a decreasing trend across the tropical Indo-Pacific).

We calculate Ω_{sw} from CESM1 LME (full forcing scenario) and LE (Representative Concentration Pathway; RCP8.5) simulated SST, SSS, pH, and DIC using CO2SYS (as described above). Combining the simulated seawater pH, DIC, and Ω with boron-derived estimates of coral calcifying fluid pH, DIC, and Ω, we estimate the percentage upregulation of calcifying fluid geochemistry. For example, the percent change (henceforth "Pchange") in aragonite saturation is calculated as:

$$\text{Pchange}_{\Omega} = \frac{\Omega_{cf} - \Omega_{sw}}{\Omega_{sw}} \times 100, \tag{5}$$

where Ω_{sw} represents the average over the time period overlapping each coral record from CESM1 LME and/or LE.

We perform sensitivity tests at the GBR site, where an *in-situ* seawater timeseries is available, to show that CESM1 LME and LE reproduce the observed Pchange_{Ω} (i.e., relative to seawater observations) to within ±26% (LME) and ±0.5% (LE), respectively (Table S8). Much of the discrepancy between LME and observed Pchange can be attributed to differences in the time periods of coverage. Therefore, two sensitivity tests were used to assess: (i) the impact of using the annual average, seasonal average (cold vs. warm season), or monthly seawater value, and (ii) the impact of using the LME projected values versus using the LE values over the post-2005 interval (i.e., after the final year of the LME). Because the Pchange seasonal variability is dominated by the variability in the coral calcifying fluid (which is $\gg$ seawater variability), these sensitivity tests demonstrate that there is no difference in the mean Pchange if the average seawater value is used in place of the observed temporal evolution of in situ Ω_{sw} (McCulloch et al., 2017). Further, this approach generates the most conservative estimate of the Pchange variability at each site (i.e., 1 σ = 23 & 32%; Table S8). The second sensitivity test demonstrated that LE-simulated seawater values displayed the best match with the in situ data over the post-2005 period ($\Delta\text{Pchange}_{\Omega} < 0.5\%$). Although there are no contemporaneous seawater samples collected near Wolf Island, Ω Pchange values using seawater data from nearby Darwin (collected in June 2012) are within the 1 σ range (±29%) of the CESM1-based estimates for WLF10-10a (ending in 2010, Table S9). We therefore conservatively reported an uncertainty of $\sim \pm 30\%$ for all Pchange_{Ω} estimates.

We also apply the method of (D'Olivo, Ellwood, et al., 2019) to deconvolve the relative contribution of thermodynamics (SST-driven changes in calcification and/or buffering capacity, (Guo, 2019)) and pH_{sw} in the observed pH_{cf} trends and seasonal variability. Briefly, we performed a multivariate linear regression between CESM1 simulated temperature and pH_{sw} (independent predictors) and pH_{cf} (dependent predictand). The sensitivity of Wolf coral pH_{cf} to SST and pH_{sw} can be expressed as:

$$\mathrm{pH}_{cf} = 0.26 \times \mathrm{pH}_{sw} - 0.0019 \times SST + 6.34, \quad (6)$$

Similar results were obtained when Sr/Ca-SSTs we used in place of CESM1 simulated SSTs. To quantify the role of SST and $\mathrm{pH_{sw}}$ in the observed trends (WLF10-10 and fossil vs. modern) and seasonal variability, we model $\mathrm{pH_{cf}}$ from Eq. 6 using either (1) the average $\mathrm{pH_{sw}}$ and simulated SST, or (2) the average SST and simulated $\mathrm{pH_{sw}}$, respectively.

Predicted changes in coral calcification

Finally, we use the IpHRAC model from (McCulloch et al., 2012) to predict the changes in calcification rate (G) from Ω_{cf} between time periods (i.e., 18^{th} and 20^{th}):

$$G = k \times (\Omega_{cf} - 1)^n, \quad (7)$$

where

$$k = -0.0177 \times SST^2 \quad (8)$$

and

$$n = 0.0628 \times SST + 0.0985. \quad (9)$$

$\mathrm{Omega_{cf}}$ is calculated from simulated pH, Ω_{sw}, SST, and SSS and the Pchange (%) upregulation, as described above. Calcification rates are reported as percent changes relative to the baseline period (1970-2005, unless otherwise noted).

Acknowledgments

We thank the Charles Darwin Station and the Parque Nacional Galápagos, particularly Galo Quezada, for field work support and permitting for coral collection. We also thank Colin Chilcott, Meriwether Wilson, Roberto Pepolas, Diego Ruiz, Jenifer Suarez, and the captain and crew of the Queen Mabel for their assistance in the field. This work is supported by National Science Foundation grants 1401326/1829613 and 0957881 to J.E.C.; UK Natural Environment Research Council grant NE/H009957/1 to A.T.; University of Arizona Honors College Alumni Legacy Grant to A.H.C.; ARC Centre of Excellence grant

CE140100020 to MM and J.P.D.; and startup funds awarded to D.T. from Boston University. AIMS is a federally funded government research agency.

Competing Interests

The authors declare that they have no competing financial interests.

Data Availability

All geochemical data will be publicly available on the National Center for Environmental Information (formerly the National Climatic Data Center) paleoclimatology database (on or before publication).

Correspondence

Correspondence and requests for materials should be addressed to D.M.T. (email: thompsod@arizona.edu).

Author contributions

J.E.C. & A.T. conceived of and funded the large coral paleoclimate effort in the Galápagos Archipelago, which motivated this work, and D.M.T., J.E.C. and M.M. conceived of this experiment. D.M.T., J.E.C., and A.T. collected the coral cores utilized in this study; D.M.T. prepared coral powders for paired boron–trace elemental analyses, including column chemistry; D.M.T., J.P.D. and K.D. conducted the geochemical analysis; D.M.T., E.V.R., A.H.C., and L.V. analyzed and compiled the longer GW10-10 modern and GW10-4 fossil records used here for comparison; D.M.T. and M.L. extracted, analyzed, and interpreted the CESM model output; D.M.T., E.V.R., J.L. and N.C collected the X-ray density measurements; D.M.T. analyzed and interpreted the data, and wrote the manuscript; and all authors provided input and contributed to finalizing and revising the manuscript.

References

Al-Horani, F., Al-Moghrabi, S., & De Beer, D. (2003). The mechanism of calcification and its relation to photosynthesis and respiration in the scleractinian coral galaxea fascicularis. *Marine Biology*, *142*(3), 419–426.

Allison, N. (2017). Reconstructing coral calcification fluid dissolved inorganic carbon chemistry from skeletal boron: An exploration of potential controls on coral aragonite b/ca. *Heliyon*, *3*(8), e00387.

Allison, N., Cohen, I., Finch, A. A., Erez, J., & Tudhope, A. W. (2014). Corals concentrate dissolved inorganic carbon to facilitate calcification. *Nature Communications*, *5*(1), 1–6.

Anderson, K. D., Cantin, N. E., Heron, S. F., Pisapia, C., & Pratchett, M. S. (2017). Variation in growth rates of branching corals along australia's great barrier reef. *Scientific reports*, *7*(1), 1–13.

Beck, J. W., Edwards, R. L., Ito, E., Taylor, F. W., Recy, J., Rougerie, F., ... Henin, C. (1992). Sea-surface temperature from coral skeletal strontium/calcium ratios. *Science*, *257*(5070), 644–647.

Burton, E. A., & Walter, L. M. (1987). Relative precipitation rates of aragonite and mg calcite from seawater: Temperature or carbonate ion control? *Geology*, *15*(2), 111–114.

Carton, J. A., & Giese, B. S. (2008). A reanalysis of ocean climate using simple ocean data assimilation (soda). *Monthly weather review*, *136*(8), 2999–3017.

Chalk, T., Standish, C., D'Angelo, C., Castillo, K., Milton, J., & Foster, G. (2021). Mapping coral calcification strategies from in situ boron isotope and trace element measurements of the tropical coral siderastrea siderea. *Scientific reports*, *11*.

Cheng, H., Edwards, R. L., Shen, C.-C., Polyak, V. J., Asmerom, Y., Woodhead, J., ... others (2013). Improvements in 230th dating, 230th and 234u half-life values, and u–th isotopic measurements by multi-collector inductively coupled plasma mass spectrometry. *Earth and Planetary Science Letters*, *371*, 82–91.

Clarke, H., D'Olivo, J., Conde, M., Evans, R., & McCulloch, M. (2019). Coral records of variable stress impacts and possible acclimatization to recent marine heat wave events on the northwest shelf of australia. *Paleoceanography and Paleoclimatology*, *34*(11), 1672–1688.

761 Clarke, H., D'Olivo, J. P., Falter, J., Zinke, J., Lowe, R., & McCulloch, M. (2017). Differential
762 response of corals to regional mass-warming events as evident from skeletal sr/ca and mg/ca
763 ratios. *Geochemistry, Geophysics, Geosystems*, *18*(5), 1794–1809.

764 Cohen, A. L., & McConnaughey, T. A. (2003). Geochemical perspectives on coral mineralization.
765 *Reviews in mineralogy and geochemistry*, *54*(1), 151–187.

766 Corrège, T., Delcroix, T., Récy, J., Beck, W., Cabioch, G., & Le Cornec, F. (2000). Evidence
767 for stronger el niño-southern oscillation (enso) events in a mid-holocene massive coral. *Pale-*
768 *oceanography*, *15*(4), 465–470.

769 Cortés, J. (1997). Biology and geology of eastern pacific coral reefs. *Coral Reefs*, *16*(1), S39–S46.

770 Darwin, C., & Bonney, T. G. (1889). *The structure and distribution of coral reefs*. Smith, Elder.

771 DeCarlo, T. M., Gaetani, G. A., Holcomb, M., & Cohen, A. L. (2015). Experimental determi-
772 nation of factors controlling u/ca of aragonite precipitated from seawater: Implications for
773 interpreting coral skeleton. *Geochimica et Cosmochimica Acta*, *162*, 151–165.

774 DeCarlo, T. M., Holcomb, M., & McCulloch, M. T. (2018). Reviews and syntheses: Revisiting the
775 boron systematics of aragonite and their application to coral calcification. *Biogeosciences*,
776 *15*(9), 2819–2834.

777 Dickson, A., & Millero, F. J. (1987). A comparison of the equilibrium constants for the dissocia-
778 tion of carbonic acid in seawater media. *Deep Sea Research Part A. Oceanographic Research*
779 *Papers*, *34*(10), 1733–1743.

780 Dickson, A. G. (1990). Thermodynamics of the dissociation of boric acid in synthetic seawater
781 from 273.15 to 318.15 k. *Deep Sea Research Part A. Oceanographic Research Papers*, *37*(5),
782 755–766.

783 Dishon, G., Fisch, J., Horn, I., Kaczmarek, K., Bijma, J., Gruber, D. F., ... Tchernov, D. (2015).
784 A novel paleo-bleaching proxy using boron isotopes and high-resolution laser ablation to
785 reconstruct coral bleaching events. *Biogeosciences*, *12*(19), 5677–5687.

786 D'Olivo, J., & McCulloch, M. (2017). Response of coral calcification and calcifying fluid composi-
787 tion to thermally induced bleaching stress. *Scientific reports*, *7*(1), 1–15.

788 D'Olivo, J. P., Ellwood, G., DeCarlo, T. M., & McCulloch, M. T. (2019). Deconvolving the
789 long-term impacts of ocean acidification and warming on coral biomineralisation. *Earth and*
790 *Planetary Science Letters*, *526*, 115785.

D'Olivo, J. P., Georgiou, L., Falter, J., DeCarlo, T. M., Irigoien, X., Voolstra, C. R., ... McCulloch, M. T. (2019). Long-term impacts of the 1997–1998 bleaching event on the growth and resilience of massive porites corals from the central red sea. *Geochemistry, Geophysics, Geosystems*, *20*(6), 2936–2954.

Edwards, R. L., Chen, J., & Wasserburg, G. (1987). 238u234u230th232th systematics and the precise measurement of time over the past 500,000 years. *Earth and Planetary Science Letters*, *81*(2-3), 175–192.

Foster, G., Pogge von Strandmann, P. A., & Rae, J. (2010). Boron and magnesium isotopic composition of seawater. *Geochemistry, Geophysics, Geosystems*, *11*(8).

Furla, P., Galgani, I., Durand, I., & Allemand, D. (2000). Sources and mechanisms of inorganic carbon transport for coral calcification and photosynthesis. *Journal of Experimental Biology*, *203*(22), 3445–3457.

Gaetani, G. A., & Cohen, A. L. (2006). Element partitioning during precipitation of aragonite from seawater: a framework for understanding paleoproxies. *Geochimica et Cosmochimica Acta*, *70*(18), 4617–4634.

Gagnon, A. C., Gothmann, A. M., Branson, O., Rae, J. W., & Stewart, J. A. (2021). Controls on boron isotopes in a cold-water coral and the cost of resilience to ocean acidification. *Earth and Planetary Science Letters*, *554*, 116662.

Gattuso, J.-P., Kirkwood, W., Barry, J., Cox, E., Gazeau, F., Hansson, L., ... others (2014). Free-ocean co2 enrichment (foce) systems: present status and future developments. *Biogeosciences (BG)*, *11*(15), 4057–4075.

Georgiou, L., Falter, J., Trotter, J., Kline, D. I., Holcomb, M., Dove, S. G., ... McCulloch, M. (2015). ph homeostasis during coral calcification in a free ocean co2 enrichment (foce) experiment, heron island reef flat, great barrier reef. *Proceedings of the National Academy of Sciences*, *112*(43), 13219–13224.

Glynn, P. (2001). Eastern pacific coral reef ecosystems. In *Coastal marine ecosystems of latin america* (pp. 281–305). Springer.

Glynn, P. W., Alvarado, J. J., Banks, S., Cortés, J., Feingold, J. S., Jiménez, C., ... others (2017). Eastern pacific coral reef provinces, coral community structure and composition: an overview. In *Coral reefs of the eastern tropical pacific* (pp. 107–176). Springer.

Glynn, P. W., Cortés-Núñez, J., Guzmán-Espinal, H. M., & Richmond, R. H. (1988). El niño (1982-83) associated coral mortality and relationship to sea surface temperature deviations in the tropical eastern pacific. mortalidad de corales asociada con el niño (1982-83) y relación con las desviaciones de la temperatura superficial del mar en el pacífico oriental tropical. In *Proceedings of the 6th international coral reef symposium, australia.* (Vol. 3, pp. 237–243).

Glynn, P. W., Feingold, J. S., Baker, A., Banks, S., Baums, I. B., Cole, J., ... others (2018). State of corals and coral reefs of the galápagos islands (ecuador): Past, present and future. *Marine pollution bulletin*, *133*, 717–733.

Guillermic, M., Cameron, L. P., De Corte, I., Misra, S., Bijma, J., de Beer, D., ... Eagle, R. A. (2020). Thermal stress reduces pocilloporid coral resilience to ocean acidification by impairing control over calcifying fluid chemistry. *Science Advances*, *7*(2), eaba9958.

Guo, W. (2019). Seawater temperature and buffering capacity modulate coral calcifying ph. *Scientific reports*, *9*(1), 1–13.

Hathorne, E. C., Felis, T., Suzuki, A., Kawahata, H., & Cabioch, G. (2013). Lithium in the aragonite skeletons of massive porites corals: A new tool to reconstruct tropical sea surface temperatures. *Paleoceanography*, *28*(1), 143–152.

Hemming, N., Guilderson, T., & Fairbanks, R. (1998). Seasonal variations in the boron isotopic composition of coral: A productivity signal? *Global biogeochemical cycles*, *12*(4), 581–586.

Holcomb, M., DeCarlo, T., Gaetani, G., & McCulloch, M. (2016). Factors affecting b/ca ratios in synthetic aragonite. *Chemical Geology*, *437*, 67–76.

Humphreys, A. F., Halfar, J., Ingle, J. C., Manzello, D., Reymond, C. E., Westphal, H., & Riegl, B. (2018). Effect of seawater temperature, ph, and nutrients on the distribution and character of low abundance shallow water benthic foraminifera in the galápagos. *PloS one*, *13*(9).

Hurrell, J. W., Holland, M. M., Gent, P. R., Ghan, S., Kay, J. E., Kushner, P., ... others (2013). The community earth system model: a framework for collaborative research. *Bulletin of the American Meteorological Society*, *94*(9), 1339–1360.

Jimenez, G., Cole, J. E., Thompson, D. M., & Tudhope, A. W. (2018). Northern Galápagos corals reveal twentieth century warming in the eastern tropical Pacific. *Geophysical Re-*

search Letters, *45*(4), 1981–1988.

Kay, J. E., Deser, C., Phillips, A., Mai, A., Hannay, C., Strand, G., ... others (2015). The Community Earth System Model (CESM) large ensemble project: A community resource for studying climate change in the presence of internal climate variability. *Bulletin of the American Meteorological Society*, *96*(8), 1333–1349.

Kessler, W. S. (2006). The circulation of the eastern tropical pacific: A review. *Progress in Oceanography*, *69*(2-4), 181–217.

Klochko, K., Kaufman, A. J., Yao, W., Byrne, R. H., & Tossell, J. A. (2006). Experimental measurement of boron isotope fractionation in seawater. *Earth and Planetary Science Letters*, *248*(1-2), 276–285.

Knebel, O., Carvajal, C., Standish, C. D., Vega, E. d. l., Chalk, T. B., Ryan, E. J., ... Kench, P. (2021). Porites calcifying fluid ph on seasonal to diurnal scales. *Journal of Geophysical Research: Oceans*, *126*(3), e2020JC016889.

Lauvset, S. K., Key, R. M., Olsen, A., van Heuven, S., Velo, A., Lin, X., ... others (2016). A new global interior ocean mapped climatology: The 1× 1 glodap version 2. *Earth System Science Data*, *8*, 325–340.

Lewis, E., Wallace, D., & Allison, L. J. (1998). *Program developed for co {sub 2} system calculations* (Tech. Rep.). Brookhaven National Lab., Dept. of Applied Science, Upton, NY (United States ....

Lough, J., & Barnes, D. (2000). Environmental controls on growth of the massive coral porites. *Journal of experimental marine biology and ecology*, *245*(2), 225–243.

Lough, J. M. (2010). Climate records from corals. *Wiley interdisciplinary reviews: climate change*, *1*(3), 318–331.

Manzello, D. (2009). Reef development and resilience to acute (el nino warming) and chronic (high-co2) disturbances in the eastern tropical pacific: a real-world climate change model. In *Proc 11th int coral reef symp* (Vol. 1, pp. 1299–1304).

Manzello, D. P. (2010). Ocean acidification hotspots: Spatiotemporal dynamics of the seawater co2 system of eastern pacific coral reefs. *Limnology and Oceanography*, *55*(1), 239–248.

Manzello, D. P. , Enochs, I. C., Bruckner, A., Renaud, P. G., Kolodziej, G., Budd, D. A., ... Glynn, P. W. (2014). Galápagos coral reef persistence after enso warming across an acidifi-

cation gradient. *Geophysical Research Letters*, *41*(24), 9001–9008.

Manzello, D. P., Kleypas, J. A., Budd, D. A., Eakin, C. M., Glynn, P. W., & Langdon, C. (2008). Poorly cemented coral reefs of the eastern tropical pacific: Possible insights into reef development in a high-co2 world. *Proceedings of the National Academy of Sciences*, *105*(30), 10450–10455.

Marchitto, T., Bryan, S., Doss, W., McCulloch, M., & Montagna, P. (2018). A simple biomineralization model to explain li, mg, and sr incorporation into aragonitic foraminifera and corals. *Earth and Planetary Science Letters*, *481*, 20–29.

Mavromatis, V., Montouillout, V., Noireaux, J., Gaillardet, J., & Schott, J. (2015). Characterization of boron incorporation and speciation in calcite and aragonite from co-precipitation experiments under controlled ph, temperature and precipitation rate. *Geochimica et Cosmochimica Acta*, *150*, 299–313.

McCulloch, M., Falter, J., Trotter, J., & Montagna, P. (2012). Coral resilience to ocean acidification and global warming through ph up-regulation. *Nature Climate Change*, *2*(8), 623–627.

McCulloch, M. T., D'Olivo, J. P., Falter, J., Holcomb, M., & Trotter, J. A. (2017). Coral calcification in a changing world and the interactive dynamics of ph and dic upregulation. *Nature communications*, *8*(1), 1–8.

McCulloch, M. T., Holcomb, M., Rankenburg, K., & Trotter, J. A. (2014). Rapid, high-precision measurements of boron isotopic compositions in marine carbonates. *Rapid Communications in Mass Spectrometry*, *28*(24), 2704–2712.

Mehrbach, C., Culberson, C., Hawley, J., & Pytkowicx, R. (1973). Measurement of the apparent dissociation constants of carbonic acid in seawater at atmospheric pressure 1. *Limnology and Oceanography*, *18*(6), 897–907.

Montagna, P., McCulloch, M., Douville, E., Correa, M. L., Trotter, J., Rodolfo-Metalpa, R., ... others (2014). Li/mg systematics in scleractinian corals: Calibration of the thermometer. *Geochimica et Cosmochimica Acta*, *132*, 288–310.

Mucci, A. (1983). The solubility of calcite and aragonite in seawater at various salinities, temperatures, and one atmosphere total pressure. *American Journal of Science*, *283*(7), 780–799.

Noireaux, J., Mavromatis, V., Gaillardet, J., Schott, J., Montouillout, V., Louvat, P., ... Neuville, D. (2015). Crystallographic control on the boron isotope paleo-ph proxy. *Earth*

and Planetary Science Letters, *430*, 398–407.

Otto-Bliesner, B. L., Brady, E. C., Fasullo, J., Jahn, A., Landrum, L., Stevenson, S., ... Strand, G. (2016). Climate variability and change since 850 CE: An ensemble approach with the Community Earth System Model. *Bulletin of the American Meteorological Society*, *97*(5), 735–754.

Pelejero, C., Calvo, E., McCulloch, M. T., Marshall, J. F., Gagan, M. K., Lough, J. M., & Opdyke, B. N. (2005). Preindustrial to modern interdecadal variability in coral reef ph. *Science*, *309*(5744), 2204–2207.

Reed, E., Thompson, D., Cole, J., Lough, J., Cantin, N., Cheung, A., ... Edwards, R. L. (2021). Impacts of coral growth on geochemistry: Lessons from the galápagos islands. *Paleoceanography and Paleoclimatology*, e2020PA004051.

Reed, E. V., Cole, J. E., Lough, J. M., Thompson, D., & Cantin, N. E. (2019). Linking climate variability and growth in coral skeletal records from the Great Barrier Reef. *Coral Reefs*, *38*(1), 29–43.

Reed, E. V., Thompson, D. M., Cole, J. E., Lough, J. M., Cantin, N. E., Cheung, A. H., ... Edwards, R. L. (2021). Impacts of coral growth on geochemistry: Lessons from the galápagos islands. *Paleoceanography and Paleoclimatology*, *36*(4), e2020PA004051.

Reynaud, S., Ferrier-Pages, C., Meibom, A., Mostefaoui, S., Mortlock, R., Fairbanks, R., & Allemand, D. (2007). Light and temperature effects on sr/ca and mg/ca ratios in the scleractinian coral acropora sp. *Geochimica et Cosmochimica Acta*, *71*(2), 354–362.

Reynolds, R. W., Rayner, N. A., Smith, T. M., Stokes, D. C., & Wang, W. (2002). An improved in situ and satellite sst analysis for climate. *Journal of climate*, *15*(13), 1609–1625.

Reynolds, R. W., Smith, T. M., Liu, C., Chelton, D. B., Casey, K. S., & Schlax, M. G. (2007). Daily high-resolution-blended analyses for sea surface temperature. *Journal of Climate*, *20*(22), 5473–5496.

Ross, C. L., DeCarlo, T. M., & McCulloch, M. T. (2019). Environmental and physiochemical controls on coral calcification along a latitudinal temperature gradient in western australia. *Global change biology*, *25*(2), 431–447.

Ross, C. L., Falter, J. L., & McCulloch, M. T. (2017). Active modulation of the calcifying fluid carbonate chemistry (δ 11 b, b/ca) and seasonally invariant coral calcification at sub-

tropical limits. *Scientific reports*, *7*(1), 1–11.

Schoepf, V., D'Olivo, J. P., Rigal, C., Jung, E. M. U., & McCulloch, M. T. (2021). Heat stress differentially impacts key calcification mechanisms in reef-building corals. *Coral Reefs*, *40*(2), 459–471.

Schoepf, V., Grottoli, A. G., Levas, S. J., Aschaffenburg, M. D., Baumann, J. H., Matsui, Y., & Warner, M. E. (2015). Annual coral bleaching and the long-term recovery capacity of coral. *Proceedings of the Royal Society B: Biological Sciences*, *282*(1819), 20151887.

Sen, S., Stebbins, J., Hemming, N., & Ghosh, B. (1994). Coordination environments of b impurities in calcite and aragonite polymorphs: a 11b mas nmr study. *American Mineralogist*, *79*(9-10), 819–825.

Sevilgen, D. S., Venn, A. A., Hu, M. Y., Tambutté, E., de Beer, D., Planas-Bielsa, V., & Tambutté, S. (2019). Full in vivo characterization of carbonate chemistry at the site of calcification in corals. *Science advances*, *5*(1), eaau7447.

Shen, C.-C., Edwards, R. L., Cheng, H., Dorale, J. A., Thomas, R. B., Moran, S. B., ... Edmonds, H. N. (2002). Uranium and thorium isotopic and concentration measurements by magnetic sector inductively coupled plasma mass spectrometry. *Chemical Geology*, *185*(3-4), 165–178.

Shen, G. T., Cole, J. E., Lea, D. W., Linn, L. J., McConnaughey, T. A., & Fairbanks, R. G. (1992). Surface ocean variability at galapagos from 1936–1982: calibration of geochemical tracers in corals. *Paleoceanography*, *7*(5), 563–588.

Spalding, M., Burke, L., Wood, S. A., Ashpole, J., Hutchison, J., & Zu Ermgassen, P. (2017). Mapping the global value and distribution of coral reef tourism. *Marine Policy*, *82*, 104–113.

Sutton, A. J., Feely, R. A., Maenner-Jones, S., Musielwicz, S., Osborne, J., Dietrich, C., ... others (2019). Autonomous seawater pco 2 and ph time series from 40 surface buoys and the emergence of anthropogenic trends. *Earth System Science Data*, 421.

Sutton, A. J., Feely, R. A., Sabine, C. L., McPhaden, M. J., Takahashi, T., Chavez, F. P., ... Mathis, J. T. (2014). Natural variability and anthropogenic change in equatorial pacific surface ocean pco2 and ph. *Global Biogeochemical Cycles*, *28*(2), 131–145.

Swart, P. K. (1983). Carbon and oxygen isotope fractionation in scleractinian corals: a review.

Earth-science reviews, *19*(1), 51–80.

Tanaka, K., Holcomb, M., Takahashi, A., Kurihara, H., Asami, R., Shinjo, R., ... McCulloch, M. (2015). Response of acropora digitifera to ocean acidification: constraints from δ 11 b, sr, mg, and ba compositions of aragonitic skeletons cultured under variable seawater ph. *Coral Reefs*, *34*(4), 1139–1149.

Wall, M., Fietzke, J., Crook, E., & Paytan, A. (2019). Using b isotopes and b/ca in corals from low saturation springs to constrain calcification mechanisms. *Nature communications*, *10*(1), 1–9.

Wall, M., Fietzke, J., Schmidt, G. M., Fink, A., Hofmann, L., De Beer, D., & Fabricius, K. (2016). Internal ph regulation facilitates in situ long-term acclimation of massive corals to end-of-century carbon dioxide conditions. *Scientific reports*, *6*, 30688.

Weber, J. N., & Woodhead, P. M. (1972). Temperature dependence of oxygen-18 concentration in reef coral carbonates. *Journal of Geophysical Research*, *77*(3), 463–473.

Zeebe, R. E., & Wolf-Gladrow, D. (2001). *Co2 in seawater: equilibrium, kinetics, isotopes* (No. 65). Gulf Professional Publishing.

Zoccola, D., Ganot, P., Bertucci, A., Caminiti-Segonds, N., Techer, N., Voolstra, C. R., ... others (2015). Bicarbonate transporters in corals point towards a key step in the evolution of cnidarian calcification. *Scientific Reports*, *5*, 9983.

Zoccola, D., Tambutté, E., Kulhanek, E., Puverel, S., Scimeca, J.-C., Allemand, D., & Tambutté, S. (2004). Molecular cloning and localization of a pmca p-type calcium atpase from the coral stylophora pistillata. *Biochimica et Biophysica Acta (BBA)-Biomembranes*, *1663*(1-2), 117–126.

Box 1. Overview of coral calcification and controls on calcifying fluid geochemistry.

Although we often think of corals as forming skeletons that directly reflect seawater chemistry, in fact corals produce their skeletons from a semi-isolated, geochemically modulated fluid, separated from seawater by a layered dermal structure. The tissue layer from which the skeleton is formed is termed the calicoblastic ectoderm, which is bathed in the calcifying fluid (cf). Here we identify the processes that control the transport of skeletal "building blocks" into the calcifying fluid and the resulting fluid geochemistry. These processes are governed by both physiological and environmental factors, and they determine the geochemistry of the skeleton (Figure 1).

1. Seawater chemistry, indicated in black, is the starting point from which the coral imports skeletal materials.
2. Passive transport (diffusion) or vacuole invagination bring seawater into the calcification environment (blue).
3. Active transport uses energy from respiration and zooxanthellar photosynthesis to drive a paracellular and trans-membrane active transport of ions. For example, alkalinity "pumps" (such as Ca-ATPase) enrich alkalinity of the fluid by transporting Ca^{2+}, $2Na^{+}$, or $2K^{+}$ while removing $2H^{+}$ (e.g., Cohen and McConnaughey 2003; Al-Horani et al., 2003; Zoccola et al., 2004; Tanaka et al., 2015). This pH increase drives the carbonate equilibrium towards CO_3^{2-}, increases alkalinity, and raises the aragonite supersaturation, enabling rapid calcification. The Ca-ATPase pump also increases the Sr^{2+} concentration of the calcifying fluid (Marchitto et al., 2018), due to strontium's similarity in size and charge to Ca^{2+}. Certain details of these active transport pathways remain obscure: although it is stimulated by light and most active during the day, it may not be energy limited (McCulloch et al. 2012), and the mechanistic links to metabolic DIC remain poorly understood (Furla et al., 2000; Zoccola et al., 2015). A strong inverse relationship between pH and DIC_{cf} (e.g., McCulloch et al., 2017) suggests that low DIC, rather than high energy, may trigger active pathways. Thus active transport can be important even when energy sources are reduced under cooler, low-light conditions. The interplay of metabolic energy supplies with external environmental stresses may vary among reef environments, and different factors may become limiting depending on these details.
4. Rayleigh fractionation alters the relative proportion of minor and trace cations to Ca in the calcifying fluid as calcification proceeds. The proxy-relevant cations Sr, Mg, Ba, Li, and U are incorporated into the coral skeleton at differing rates due to varying partitioning coefficients. Calcification preferentially incorporates Sr and Ba, and discriminates against Mg, Li, and U, relative to the proportion of these elements in the cf. The degree to which Rayleigh fractionation impacts the cf chemistry will depend on the balance between calcification rate, which increasingly fractionates cf chemistry, and replenishment of seawater, which brings cf chemistry back to environmental levels. The susceptibility of different elements to this process depends on the partitioning coefficient (K_D) between fluid and aragonite during calcification, with values <1 indicating exclusion from the skeleton and those >1, preferential uptake: K(Sr/Ca) ~ 1.1 (Gaetani et al., 2006; Marchitto et al., 2018), K(Mg/Ca) ~ 0.001 (Gaetani et al., 2006), K(Ba/Ca) ~2.3 (Gaetani et al., 2006), K(Li/Ca) ~ 0.0006 (Hathorne et al., 2013), K(U/CO3) ~ 0.3 (DeCarlo et al., 2015)].

Figure 1.

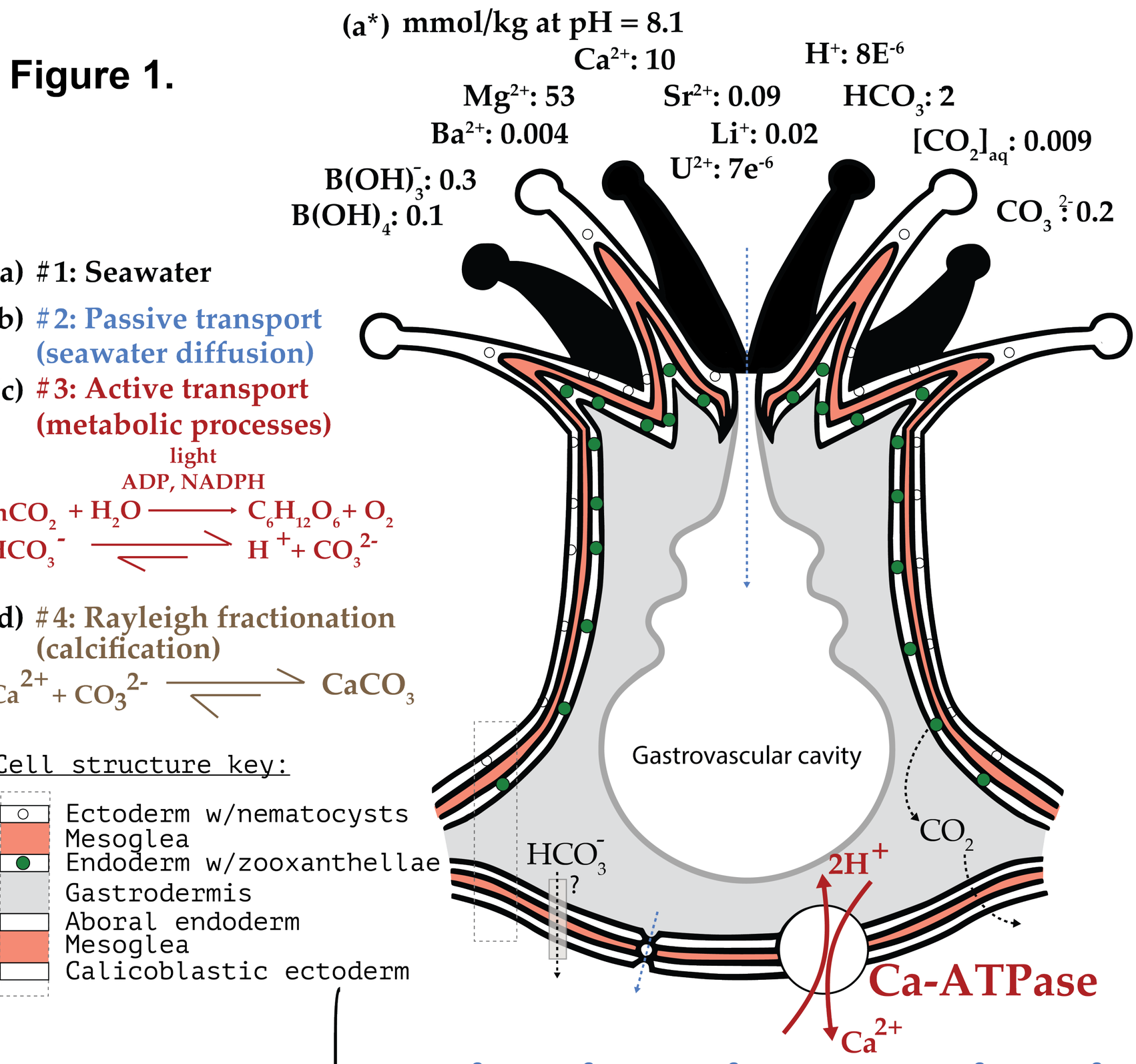

For major cations and anions in Figure 1, the notation is as follows:

(a*) concentration in seawater at a pH (total scale) of 8.1 (in mmol/kg, rounded to one significant figure);

(b*) as in (a*), due to 1:1 passive transport of ions, but now expressed as stoichiometric ratios with respect to 1 mole of $CaCO_3$ (ions in curly brackets are thought to play a minor role in coral carbonate reactions);

(c*) the relative impact of Ca-ATPase pump on calcifying fluid geochemistry, where known (McCulloch et al., 2017; Marchitto et al., 2018);

(d*) impact of calcification on the concentration of major cations whose substitution for Ca^{2+} is used for paleo proxy(ies), based on the partitioning of each between the fluid and aragonite phases (Gaetani et al., 2006; Marchitto et al., 2018; Hathorne et al., 2013; DeCarlo et al., 2015).

DIC = Dissolved Inorganic Carbon;
TA = Total Alkalinity. Diagram not to scale.
See Table S1 for a list of geochemical proxies analyzed in this study, and their interpretation.

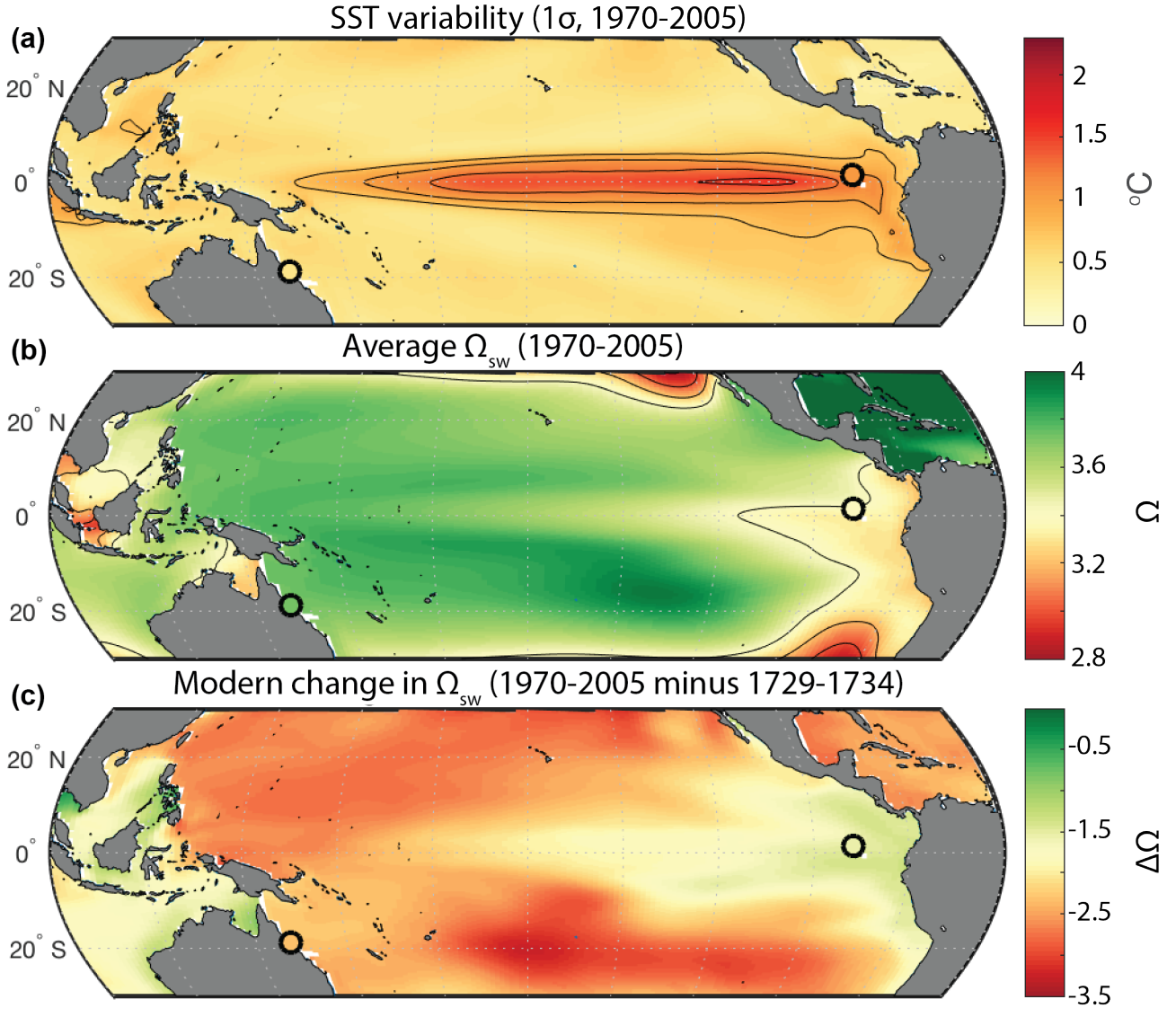
(a)
SST variability (1σ, 1970-2005)
20° N
0°
20° S
2
1.5
1
0.5
0
°C
(b)
Average Ω sw (1970-2005)
20° N
0°
20° S
4
3.6
3.2
2.8
Ω
(c)
Modern change in Ω sw (1970-2005 minus 1729-1734)
20° N
0°
20° S
-0.5
-1.5
-2.5
-3.5
ΔΩ

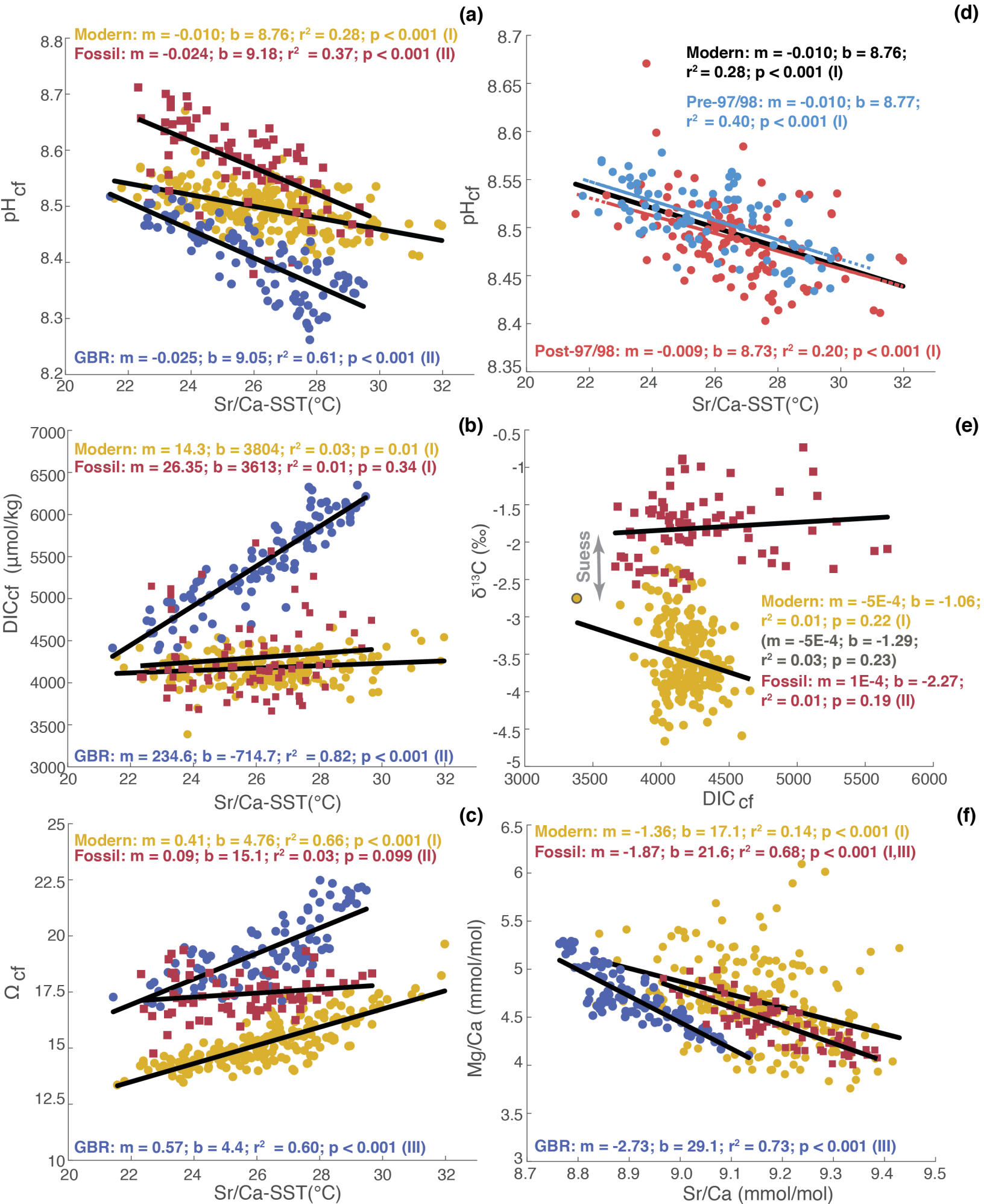
(a)
Modern: m = -0.010; b = 8.76; r² = 0.28; p < 0.001 (I)
Fossil: m = -0.024; b = 9.18; r² = 0.37; p < 0.001 (II)
GBR: m = -0.025; b = 9.05; r² = 0.61; p < 0.001 (II)
pHcf
Sr/Ca-SST(°C)
(d)
Modern: m = -0.010; b = 8.76;
r² = 0.28; p < 0.001 (I)
Pre-97/98: m = -0.010; b = 8.77;
r² = 0.40; p < 0.001 (I)
Post-97/98: m = -0.009; b = 8.73; r² = 0.20; p < 0.001 (I)
pHcf
Sr/Ca-SST(°C)
(b)
Modern: m = 14.3; b = 3804; r² = 0.03; p = 0.01 (I)
Fossil: m = 26.35; b = 3613; r² = 0.01; p = 0.34 (I)
GBR: m = 234.6; b = -714.7; r² = 0.82; p < 0.001 (II)
DICcf (µmol/kg)
Sr/Ca-SST(°C)
(e)
Suess
Modern: m = -5E-4; b = -1.06;
r² = 0.01; p = 0.22 (I)
(m = -5E-4; b = -1.29;
r² = 0.03; p = 0.23)
Fossil: m = 1E-4; b = -2.27;
r² = 0.01; p = 0.19 (II)
δ13C (‰)
DIC cf
(c)
Modern: m = 0.41; b = 4.76; r² = 0.66; p < 0.001 (I)
Fossil: m = 0.09; b = 15.1; r² = 0.03; p = 0.099 (II)
GBR: m = 0.57; b = 4.4; r² = 0.60; p < 0.001 (III)
Ω cf
Sr/Ca-SST(°C)
(f)
Modern: m = -1.36; b = 17.1; r² = 0.14; p < 0.001 (I)
Fossil: m = -1.87; b = 21.6; r² = 0.68; p < 0.001 (I,III)
GBR: m = -2.73; b = 29.1; r² = 0.73; p < 0.001 (III)
Mg/Ca (mmol/mol)
Sr/Ca (mmol/mol)

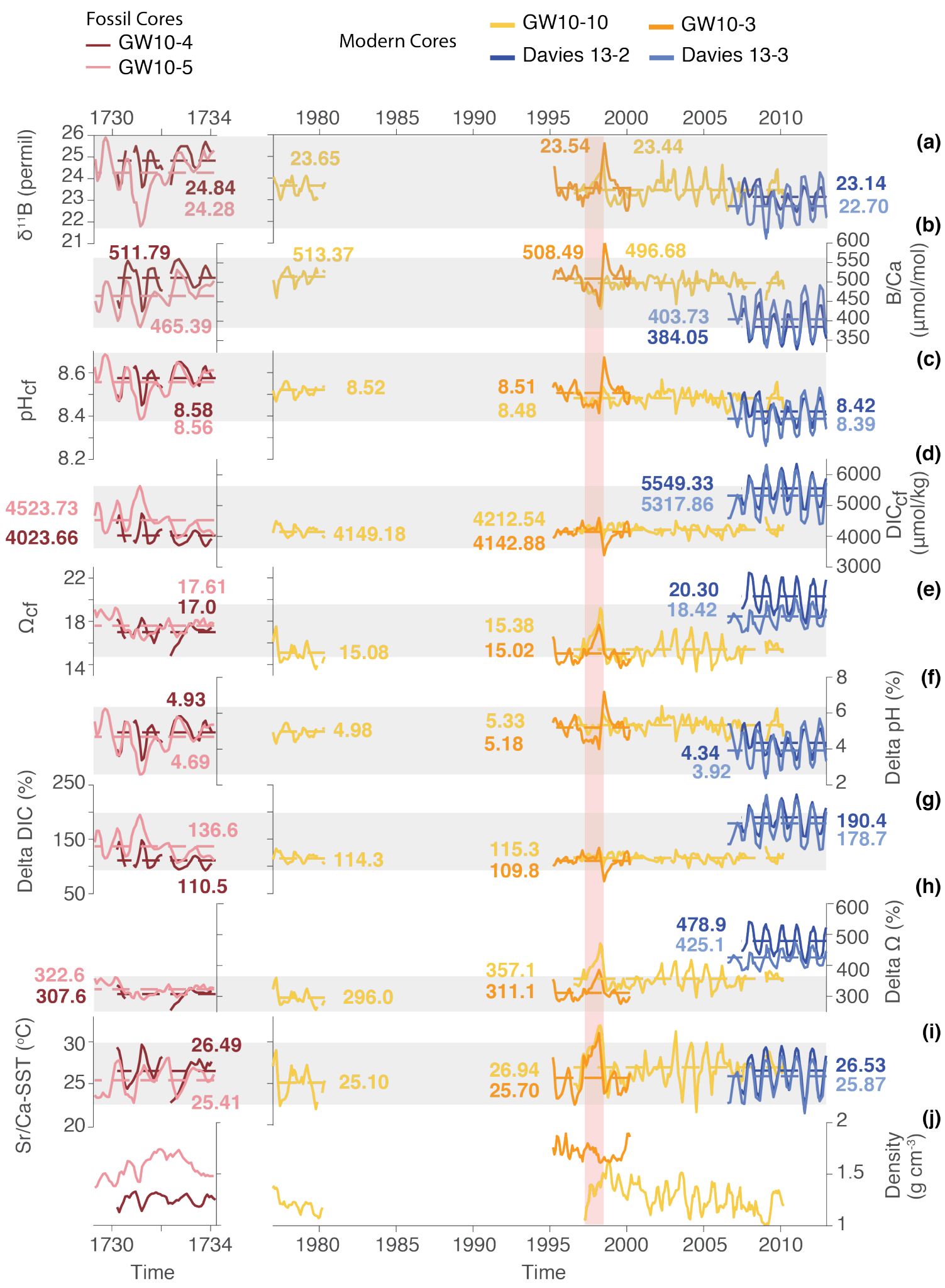
Fossil Cores
GW10-4
GW10-5
Modern Cores
GW10-10
GW10-3
Davies 13-2
Davies 13-3
1730
1734
1980
1985
1990
1995
2000
2005
2010
(a)
δ11B (permil)
26
25
24
23
22
21
24.84
24.28
23.65
23.54
23.44
23.14
22.70
(b)
B/Ca (µmol/mol)
600
550
500
450
400
350
511.79
465.39
513.37
508.49
496.68
403.73
384.05
(c)
pHcf
8.6
8.4
8.2
8.58
8.56
8.52
8.51
8.48
8.42
8.39
(d)
DICcf (µmol/kg)
6000
5000
4000
3000
4523.73
4023.66
4149.18
4212.54
4142.88
5549.33
5317.86
(e)
Ωcf
22
18
14
17.61
17.0
15.08
15.38
15.02
20.30
18.42
(f)
Delta pH (%)
8
6
4
2
4.93
4.69
4.98
5.33
5.18
4.34
3.92
(g)
Delta DIC (%)
250
150
50
136.6
110.5
114.3
115.3
109.8
190.4
178.7
(h)
Delta Ω (%)
600
500
400
300
322.6
307.6
296.0
357.1
311.1
478.9
425.1
(i)
Sr/Ca-SST (°C)
30
25
20
26.49
25.41
25.10
26.94
25.70
26.53
25.87
(j)
Density (g cm-3)
2
1.5
1
Time
Time